

## MASS MODELING OF DISK GALAXIES: DEGENERACIES, CONSTRAINTS AND ADIABATIC CONTRACTION

AARON A. DUTTON

Department of Physics & Astronomy, University of British Columbia, 6224 Agricultural Road, Vancouver,  
BC V6T 1Z1, Canada; and Institute of Astronomy, Department of Physics, ETH Zürich,  
Scheuchzerstrasse 7, 8093 Zürich, Switzerland; dutton@phys.ethz.ch

STÉPHANE COURTEAU

Department of Physics, Queen's University, Kingston ON, K7L 3N6, Canada; courteau@astro.queensu.ca

ROELOF DE JONG

Space Telescope Science Institute, 3700 San Martin Dr., Baltimore, MD 21218, USA; dejong@stsci.edu

AND

CLAUDE CARIGNAN

Département de Physique, Université de Montréal, C.P. 6128, Station Centre-Ville, Montréal,  
QC H3C 3J7, Canada; carignan@astro.umontreal.ca

Received 2003 september 30; accepted 2004 September 15

### ABSTRACT

This paper addresses available constraints on mass models fitted to rotation curves. Mass models of disk galaxies have well-known degeneracies, that prevent a unique mass decomposition. The most notable is due to the unknown value of the stellar mass-to-light ratio (the disk-halo degeneracy); even with this known, degeneracies between the halo parameters themselves may prevent an unambiguous determination of the shape of the dark halo profile, which includes the inner density slope of the dark matter halo. The latter is often referred to as the “cusp-core degeneracy.” We explore constraints on the disk and halo parameters and apply these to four mock and six observed disk galaxies with high resolution and extended rotation curves. Our full set of constraints consists of mass-to-light ( $M/L$ ) ratios from stellar population synthesis models based on  $B-R$  colors, constraints on halo parameters from  $N$ -body simulations, and constraining the halo virial velocity to be less than the maximum observed velocity. These constraints are only partially successful in lifting the cusp-core degeneracy. The effect of adiabatic contraction of the halo by the disk is to steepen cores into cusps and reduce the best-fit halo concentration and  $M/L$  values (often significantly). We also discuss the effect of disk thickness, halo flattening, distance errors, and rotation curve error values on mass modeling. Increasing the imposed minimum rotation curve error from typically low, underestimated values to more realistic estimates decreases the  $\chi^2$  substantially and makes distinguishing between a cuspy or cored halo profile even more difficult. In spite of the degeneracies and uncertainties present, our constrained mass modeling favors sub-maximal disks (i.e., a dominant halo) at 2.2 disk scale lengths, with  $V_{\text{disk}}/V_{\text{tot}} \lesssim 0.6$ . This result holds for both the un-barred and weakly barred galaxies in our sample.

*Subject headings:* dark matter — galaxies: fundamental parameters — galaxies: halos — galaxies: kinematics and dynamics — galaxies: spiral — galaxies: structure

### 1. INTRODUCTION

There has been significant debate recently about the shape of dark matter density profiles, especially regarding their inner slope,  $\alpha$ .<sup>1</sup> Based on cosmological  $N$ -body simulations (Navarro, Frenk, & White 1996; Navarro, Frenk, & White 1997; hereafter NFW), the dark matter halo profile appears to be independent of mass and has an inner logarithmic slope  $\alpha = 1$ . More recent, higher resolution simulations suggest that the density profiles do not converge to a single power-law at small radii. At the smallest resolved scales ( $\approx 0.5\%$  of the virial radius) profiles usually have slopes between 1 and 1.5 (Moore et al. 1999; Ghigna et al. 2000; Jing & Suto 2000; Fukushige & Makino 2001; Klypin et al. 2001; Power et al. 2003; Navarro et al. 2004; Diemand et al. 2004).

<sup>1</sup> Values of  $\alpha$  range from 0 (core) to 1.5 (cuspy). We define the dark matter profile and  $\alpha$  in Equation (4).

At large radii all simulations find density profiles with slopes  $\alpha \approx -3$ , which is *inconsistent* with the isothermal ( $\rho \propto r^{-2}$ ) profile. The determination of the dark halo slope based on mapping the outer density profile of galaxies is difficult, owing mainly to a lack of mass tracers at large radii. Prada et al. (2003) find that the line-of-sight velocity dispersion of satellite galaxies declines with distance to the primary, in agreement with a  $\rho \propto r^{-3}$  density profile at large radii.

The determination of  $\alpha$  based on data at smaller radii is complicated by the unknown value of the stellar mass-to-light ratio,  $\Upsilon_d$ . This has led to dedicated analyses on dwarf<sup>2</sup> and low surface brightness<sup>3</sup> (LSB) galaxies that are believed to be

<sup>2</sup> Dwarf spiral galaxies are usually defined as having a maximum rotation velocity  $v_{\text{max}} < 100 \text{ km s}^{-1}$  and/or a total magnitude  $M_B \geq -18$ .

<sup>3</sup> An LSB galaxy is usually defined as a disk galaxy with an extrapolated central disk surface brightness  $\mu_0^B$  roughly 2 mag arcsec<sup>-2</sup> fainter than the typical value for HSB galaxies of  $\mu_0^B = 21.65$  (Freeman 1970).

dark matter dominated at all radii (de Blok & McGaugh 1997; Verheijen 1997; Swaters 1999).

It has been suggested that rotation curves of dwarf and LSB galaxies rise less steeply than predicted by numerical simulations based on the cold dark matter (CDM) paradigm (Moore 1994; Flores & Primack 1994; de Blok & McGaugh 1997; McGaugh & de Blok 1998; de Blok et al. 2001a,b). However, a number of observational uncertainties cast doubt over these early conflicting claims. These include beam smearing for HI rotation curves (Swaters et al. 2000; van den Bosch et al. 2000), high inclination angles and H $\alpha$  long-slit alignment error (Swaters et al. 2003a), and non-circular motions close to the center of galaxies (Swaters et al. 2003b). Many of these uncertainties can be quantified or eliminated by measuring high-resolution two-dimensional velocity fields (Barnes, Sellwood, & Kosowsky 2004). At optical wavelengths, these can be obtained via Fabry-Perot interferometry (e.g., Blais-Ouellette et al. 1999) or integral field spectroscopy (e.g., Andersen & Bershad 2003; Courteau et al. 2003).

Despite a low ratio of baryonic to non-baryonic matter in dwarf and LSB galaxies, practical limitations in accurately determining the circular velocity profile have prevented a reliable determination of the dark matter density profile for those galaxies. Furthermore, the predictions of numerical simulations are weakest on the (small) scales of dwarf and LSB galaxies. By comparison, for high surface brightness (HSB) galaxies the kinematics is easier to measure and the expected dark halos can be better resolved in numerical simulations, but the more prominent stellar component often hinders a unique mass decomposition.

In principle, if the disk mass-to-light ratio,  $\Upsilon_d$ , and the gaseous mass distribution are known, the contribution from the dark halo to the overall potential can be determined. However, extracting the parametrized halo profile with this procedure is complicated owing to a degeneracy between the halo parameters themselves (e.g., van den Bosch & Swaters 2001). Furthermore, various evolutionary processes may alter the dark halo density profile from that found in dark matter-only simulations. The dissipation of the disk is thought to compress the dark halo distribution through adiabatic contraction (Blumenthal et al. 1986; Flores et al. 1993), while other processes such as feedback, mergers, spin segregation (Maller & Dekel 2002; Dekel et al. 2003), pre-processing of dark halos (Mo & Mao 2003), and bar-driven dark halo evolution (Weinberg & Katz 2002) are thought to lower the concentration and central cusp of dark matter halos.

In this paper we discuss and apply mass modeling constraints in an attempt to break internal modeling degeneracies and thus determine the best parameterization of the dark halo. We present our mass models in §2 and their degeneracies in §3. The mass model constraints are presented in §4. We then apply these constraints to six galaxies from Blais-Ouellette (2000). The data are presented in §5, and the models are applied to the data in §6. The effects of rotation curve errors, distance, disk thickness, and halo flattening are discussed in §7, and a summary is offered in §8.

Throughout this paper  $r$  and  $R$  refer to the radius from the galaxy center in spherical and cylindrical coordinates, respectively. Whenever necessary, we also adopt a value of the Hubble constant<sup>4</sup>  $H_0$  given by  $h = H_0/100 = 0.7$ .

<sup>4</sup> The current best estimate of the Hubble constant is  $H_0 = 72 \pm 8 \text{ km s}^{-1} \text{ Mpc}^{-1}$  (*HST*  $H_0$  Key Project; Freedman et al. 2001).

## 2. MASS MODELS

Our mass models consist of three main components for each disk galaxy: a thick stellar disk (hereafter the “disk”), an infinitesimally thin gas disk (hereafter the “gas”), and an oblate dark halo (hereafter the “halo”). In general, disk galaxies may also have a bulge component, although for simplicity we limit our analysis to nearly bulge-less systems. Assuming that the matter distribution is axially symmetric and in virial equilibrium, the total circular velocity is given by

$$V_{\text{circ}} = \sqrt{V_{\text{gas}}^2 + V_{\text{disk}}^2 + V_{\text{halo}}^2}, \quad (1)$$

at each radius  $R$ . Each of the three components is described in more detail below. We compute the circular velocities of the disk and gas using formula A.17 of Casertano (1983). The best-fitting mass model is determined by fitting  $V_{\text{circ}}$  to the observed circular rotation velocity,  $V_{\text{rot}}$ , by minimizing the  $\chi^2$ -statistic with a non-linear optimization scheme.

### 2.1. Stellar Disk

We model the disk with the following density profile (van der Kruit & Searle 1981):

$$\rho_{\text{disk}}(R, z) = \frac{\Sigma(R) \text{sech}^2(z/z_0)}{2z_0}, \quad (2)$$

where  $\Sigma(R)$  is the disk surface density profile and  $z_0$  is the vertical scale height. Unless otherwise stated, we compute  $\Sigma(R)$  from the observed surface brightness profile.

The vertical scale height is parameterized in terms of the intrinsic disk thickness,  $q_d \equiv z_0/R_d$ , where  $R_d$  is the disk scale length. Unless otherwise stated, we adopt  $q_d = 0.25$  (Kregel et al. 2002; Bizyaev & Mitronova 2002). We explore the effect of disk thickness in §7.

### 2.2. Gaseous Disk

We model the gas disk with the following density profile:

$$\rho_{\text{gas}}(R, z) = \delta(z) \Sigma_{\text{HI}}(R) / f_{\text{HI}} \quad (3)$$

where  $\delta(z)$  is the Kronecker delta function,  $\Sigma_{\text{HI}}(R)$  is the surface density of neutral hydrogen, and  $f_{\text{HI}}$  is the fraction of gas in HI. We adopt  $f_{\text{HI}} = 0.75$  (e.g., Blais-Ouellette et al. 2001); other authors take  $0.71 \leq f_{\text{HI}} \leq 0.77$ , although the exact value is not critical.

Some spiral galaxies show a central depression in the HI density, likely due to the gas being present in a different form (ionized or molecular) and/or partially or completely consumed in previous episodes of star formation. A central depression and hence a positive radial density gradient result in an outward radial force or negative  $V_{\text{gas}}^2$ . We represent this as negative velocity on the gaseous component of the rotation curve.

### 2.3. Dark Halo

To take account of the uncertainties in the predicted inner halo density profiles and to allow for halos with flat central density profiles while preserving the  $\rho \propto r^{-3}$  dependence at large radii, we use the following density profile (hereafter ALP profile; Kravtsov et al. 1998):

$$\rho_{\text{halo}}(r) = \frac{\rho_0}{(r/r_s)^\alpha (1+r/r_s)^{3-\alpha}}. \quad (4)$$

This density profile has an inner logarithmic slope of  $-\alpha$  and an outer logarithmic slope of  $-3$ . For  $\alpha = 1$  this reduces to

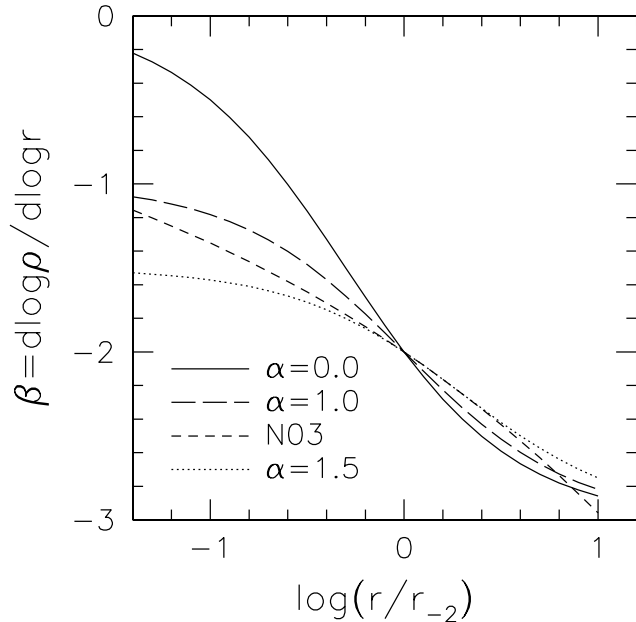


FIG. 1.— Logarithmic slope of the ‘ALP’ halo density profiles for  $\alpha = 0, 1,$  and  $1.5$  and  $c = 10$  plotted from  $0.4\% r_{200} \leq r \leq r_{200}$ . The highest resolution  $N$ -body simulations can resolve the density profile over this range. Typical density profiles lie between the  $\alpha = 1$  and  $\alpha = 1.5$  lines. For comparison with the ‘ALP’ parameterization we show the fitting function of Navarro et al. 2004.

the NFW profile, and at the scale radius,  $r_s$ , the slope of the density profile is  $-2$ .

However, for different values of  $\alpha$ ,  $r_s$  corresponds to different density slopes. To enable an easier comparison of scale radii, we replace  $r_s$  with  $r_{-2}$ , the radius where the slope of the density profile is  $-2$ . With the conversion  $r_{-2} \equiv (2 - \alpha)r_s$ .

Figures 1, 2, and 3 show the logarithmic density slopes, density profiles, and circular velocity profiles for halos with  $\alpha = 0, 1,$  and  $1.5$  and the fitting function from Navarro et al. 2004 (which has effectively  $\alpha \simeq 1.2$ ).

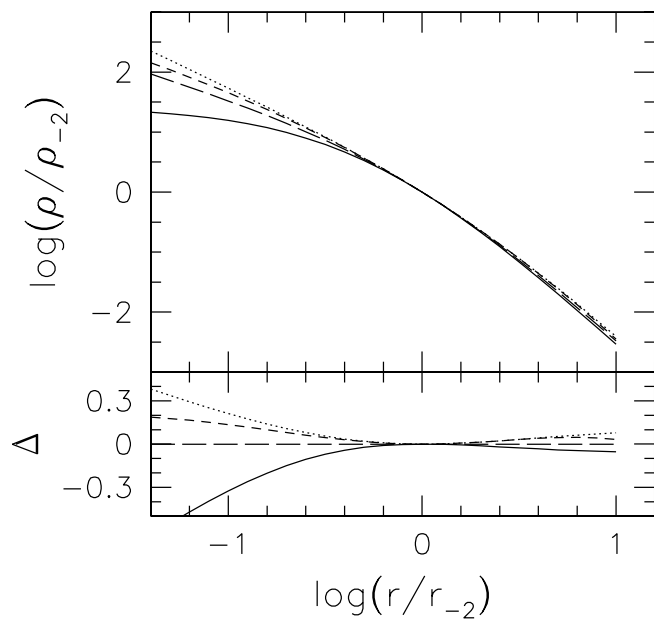


FIG. 2.— Density profiles for halos in Fig. 1 normalized to the density at the scale radius,  $\rho_{-2}$ . The bottom panel shows the differences with respect to the  $\alpha = 1$  profile.

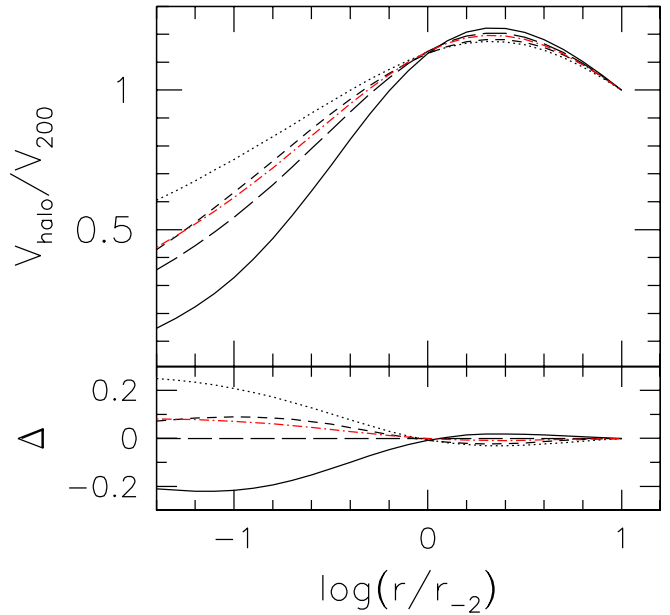


FIG. 3.— Circular velocity profiles for halos in Fig. 1 normalized to the virial velocity,  $V_{200}$ . The bottom panel shows the differences with respect to the  $\alpha = 1$  profile. Note that the differences between the profiles are most conspicuous for radii less than  $\sim 0.5 r_{-2}$ . Also shown is a halo with  $\alpha = 1.2$  (red dot-dashed line), which is effectively indistinguishable from the Navarro et al. (2004) fitting function.

### 2.3.1. Oblate/Prolate Density Profiles

Typically rotation curve analyses assume a spherical dark halo even though CDM simulations suggest triaxial shapes for collapsed structures, with typical axis ratios  $c/a = 0.5 - 0.7$  and  $b/a = 0.7 - 0.9$  (Dubinski & Carlberg 1991; Jing & Suto 2002; Tinker & Ryden 2002). However, the dissipative infall of gas in non-baryonic dark halos suppresses triaxial structures, leading to halos with an oblate shape (Katz & Gunn 1991; Dubinski 1994; although further investigation is needed to quantify this effect).

This tentative conclusion agrees with a variety of observations that find axially symmetric disks, with eccentricity  $e < 0.05$  ( $b/a > 0.9987$ ; Combes 2002 and references therein). The flattening of the halo is not easily measured, but various techniques, including the flaring of HI disks, polar rings around spiral galaxies, and X-ray isophotes of elliptical galaxies, suggest oblate halos with an axis ratio,  $q = c/a$ , ranging from 0.1 to 0.9 (Combes 2002).

Thus, we are compelled to study the effects of axially symmetric dark halos ( $b/a = 1$ ) in our mass models. We generalize the density profiles to the family of axially symmetric ellipsoids by setting  $\rho(r) = \rho(m)$ , where  $m^2 = R^2 + z^2/q^2$ .

### 2.3.2. $c - V_{200}$ parameterization

We choose to parameterize the density profile by the circular velocity at the virial radius,  $V_{\text{vir}}$ , and the concentration parameter,  $c_{-2} = R_{\text{vir}}/r_{-2}$ . Here  $R_{\text{vir}}$  is the virial radius in the  $z = 0$  plane. We choose to define the virial radius,  $R_{\text{vir}}$ , as the radius where the mean density of the halo is  $\Delta_{\text{vir}}$  times the critical density,

$$\bar{\rho}(m_{\text{vir}}) = \frac{M(m_{\text{vir}})}{\frac{4}{3}\pi q m_{\text{vir}}^3} = \Delta_{\text{vir}} \rho_{\text{crit}}, \quad (5)$$

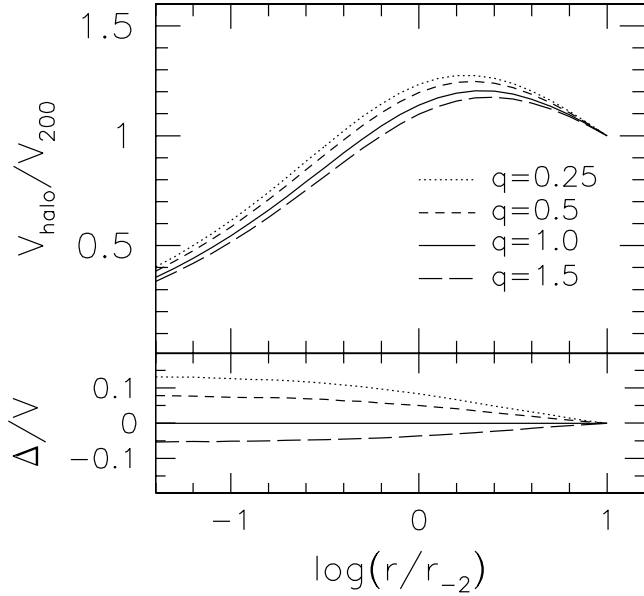


FIG. 4.— Effect of halo flattening  $q$  on circular velocity profiles for  $\alpha = 10$  halos with  $c = 10$ . The bottom panel shows the fractional differences with respect to the  $q = 1$  case. Note that these differences increase with decreasing radii.

where  $\rho_{\text{crit}} = \frac{3H^2}{8\pi G}$  is the critical density of the universe. With these definitions  $m_{\text{vir}}$ , and hence  $R_{\text{vir}}$ , will be invariant under changes of  $q$ . Unless otherwise stated, we adopt  $\Delta_{\text{vir}} = 200$ , although in currently favored  $\Lambda$ CDM cosmologies, at redshift zero, the virial radius occurs at  $\Delta_{\text{vir}} = 337 \Omega_M \simeq 100$  (Bryan & Norman 1998). The choice of  $\Delta_{\text{vir}}$  does not affect the density profile, but the virial radius changes by a factor of  $\sim 1.3$ .

With these definitions and using Equation 2.91 in Binney & Tremaine (1987) for the computation of  $V_{\text{circ}}$ , the velocity contribution of the halo specified by  $V_{200}$ ,  $c_{-2}$ ,  $\alpha$ , and  $q$  is given by

$$V_{\text{halo}}^2(x, z=0) = V_{200}^2 \frac{\mu(x, \alpha, q)/x}{\mu(c_{-2}, \alpha, q)/c_{-2}}, \quad x = R/r_{-2} \quad (6)$$

where

$$\mu(x, \alpha, q) = \int_0^x \frac{y^{2-\alpha} [1 - (2-\alpha)y]^{\alpha-3}}{\sqrt{1 - (1-q^2)y^2/x^2}} dy. \quad (7)$$

With the above definitions we can express the relationship between  $R_{\text{vir}}$  and  $V_{\text{vir}}$  as

$$\left(\frac{V_{\text{vir}}}{R_{\text{vir}}}\right)^2 = h^2 \left(\frac{\Delta_{\text{vir}}}{200}\right) \frac{\mu(c_{-2}, \alpha, q)}{\mu(c_{-2}, \alpha, 1)} \quad (8)$$

with  $V_{\text{vir}}$  and  $R_{\text{vir}}$  in  $\text{km s}^{-1}$  and kpc, respectively, and  $h = H_0/100 = 0.7$ .

Fig. 4 shows the effect of  $q$  on the circular velocity of the halo, normalized by  $V_{\text{vir}}$ . Note that for a given  $R_{\text{vir}}$ ,  $c_{-2}$ , and  $\alpha$ ,  $V_{\text{vir}}$  increases as  $q$  decreases. Oblate ( $q < 1$ ) halos result in higher circular velocities, especially near the center, while prolate ( $q > 1$ ) halos result in lower circular velocities.

### 2.3.3. Adiabatic Contraction

We model the response of the dissipation-less halo to the infall of the dissipational baryons as they cool and settle into a disk following Blumenthal et al. (1986) and Flores et al. (1993). This assumes that the collapse of the baryons

is slow, the matter distribution is spherically symmetric, and particles move on circular orbits. Then the adiabatic invariant is simply  $rM(r)$ , where  $M(r)$  is the mass enclosed by radius  $r$ . With the further assumptions that the dark matter particles do not cross orbits,  $M_{\text{DM}}(r_f) = M_{\text{DM}}(r_i)$ , where  $r_i$  and  $r_f$  are the initial and final radii of the disk, respectively, and that the baryons are initially mixed with the dark matter with a baryon fraction  $f_B = M_B/(M_B + M_{\text{DM}})$ , then given the *initial* dark halo distribution  $M_{\text{DM}}(r_i)$  and final baryonic mass distribution  $M_B(r_f)$ , the final radius,  $r_f$ , can be obtained by solving

$$r_f [M_B(r_f) + M_{\text{DM}}(r_f)] = r_i M_{\text{DM}}(r_i) / (1 - f_B). \quad (9)$$

We obtain the baryonic mass from the observations of stars and gas in the disk (§2.1), for a given  $\Upsilon_d$  and distance, and assume that the fraction of baryons in the halo is negligible. For the mass of the halo we assume the virial mass,  $M_{\text{vir}}$ .

The effect of adiabatic contraction on the density and circular velocity distributions can be quite substantial. We illustrate this effect in Figure 5. This shows the circular velocity of the initial and final halo and final disk. Here the disk is exponential with  $R_d = 2 \text{ kpc}$ ,  $\mu_0^R = 20 \text{ mag arcsec}^{-2}$  ( $R$ -band), and  $\Upsilon_d^R = 1.0$  and  $0.25$ . The effect of adiabatic contraction is largest for halos with low values of  $\alpha$  and  $c_{-2}$ , such that *halos with initial cores end up with cusps*. For very cuspy halos, the halo can expand in the very center, as the final baryonic mass within  $r_i$  is less than the initial baryonic mass within  $r_i$ . Note that although the mass is more centrally concentrated after adiabatic contraction, the formal concentration,  $c_{-2}$ , can stay the same.

Despite the simplifying assumptions, the validity of the adiabatic approximation of Blumenthal et al. (1986) has been confirmed down to  $10^{-2} r_{-2}$  in a study of the response of a dark matter halo to the growth of an exponential disk in high-resolution  $N$ -body simulations (Jesseit et al. 2002). However, Wilson (2003) and Gnedin et al. (2004) claim that under more general conditions the standard model for adiabatic contraction systematically overpredicts the contraction in the innermost regions, while slightly underpredicting the contraction at larger radii. Therefore, we use the standard model for adiabatic contraction to provide an upper limit on the effect of adiabatic contraction.

### 3. MODEL DEGENERACIES

Several degeneracies exist between the model parameters, which may prevent a unique mass decomposition. These can be divided into “disk-halo” and “cusp-core” degeneracies.

The “disk-halo” degeneracy occurs between  $\Upsilon_d$  and the halo parameters. Equally good fits, in a  $\chi^2$ -statistical sense, where  $\chi_r^2$  is the reduced- $\chi^2$ , can be obtained with a wide range of  $\Upsilon_d$  from zero to a maximum disk (e.g., van Albada et al. 1985). To break this degeneracy, we need a priori knowledge of  $\Upsilon_d$ , or  $V_{\text{disk}}/V_{\text{tot}}$ . If the disk thickness and halo flattening are ignored, this fixes the density profile of the dark halo. However, in practice, with errors on the circular velocities of a few kilometers per second finite spatial resolution, and limited extent of the rotation curve, degeneracies between the halo parameters themselves often prevent a unique parameterization of the halo density profile (van den Bosch & Swaters 2001). To break this degeneracy, constraints need to be placed on  $c_{-2}$  and  $V_{200}$  as well.

We illustrate these degeneracies with mock rotation curves. Our mock galaxies consist of an exponential disk specified by  $\mu_0^R = 20 \text{ mag arcsec}^{-2}$ ,  $R_d = 2 \text{ kpc}$ , and  $\Upsilon_d^R = 1$  and an adiabatically contracted dark halo with initial parameters  $c_{-2} = 10$ ,

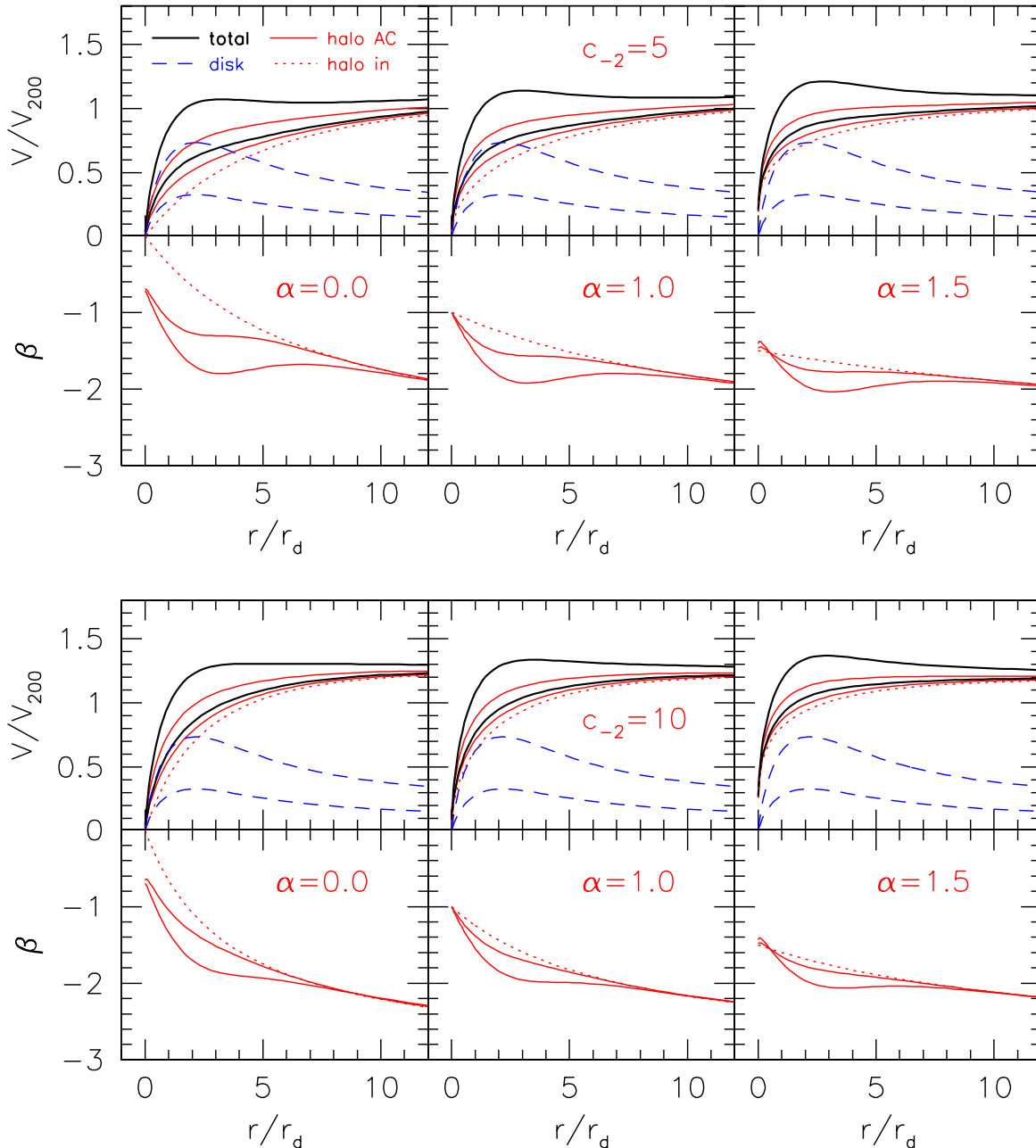


FIG. 5.— Effect of adiabatic contraction on circular velocity and halo density slopes for halos with  $\alpha=0, 1.0$ , and  $1.5$  (left to right),  $c_{-2} = 5$  (top) and  $10$  (bottom), for exponential disks with  $R_d = 2$  kpc and  $\Sigma_0 = 258$  and  $52 M_\odot \text{pc}^{-2}$ . For each disk-halo system we show the initial halo (red dotted line), final halo after adiabatic contraction (AC; red solid line), disk (blue dashed), and final total circular velocity (black thick solid).

$V_{200} = 100 \text{ km s}^{-1}$ , and  $\alpha = 0, 0.5, 1$ , and  $1.5$ . We then sample the rotation curve in  $3''$  bins up to  $2R_d$  and in  $15''$  bins up to  $8R_d$  to simulate H $\alpha$  and HI data respectively. We then add a random Gaussian error (with  $\sigma = 4 \text{ km s}^{-1}$ ) and assign a conservative measurement error of  $4 \text{ km s}^{-1}$  to each data point.

We fit for  $c_{-2}$  and  $V_{200}$  on a grid of  $\alpha$  and  $\Upsilon_d^R$ , with and without adiabatic contraction. The results of these fits are shown in Fig. 6. The disk-halo and cusp-core degeneracies exist for all input values of  $\alpha$  and are strongest for  $\alpha = 1$  halos. Thus, for these model galaxies, *without constraints it is impossible to determine  $\Upsilon_d^R$  or  $\alpha$  based on the  $\chi_r^2$  value alone.* When fitting without adiabatic contraction, a wider range of  $\Upsilon_d^R$  is

permitted, including maximum disks for  $\alpha = 0$  halos. We also see that the form of the  $c_{-2} - \alpha$  relation is the same for all fits, but the normalization is lower for fits with adiabatic contraction and a higher input  $\alpha$ .

In order to achieve reliable results out of the mass modeling exercise, we must therefore consider independent constraints, which we discuss below.

#### 4. CONSTRAINTS

##### 4.1. Stellar Population Synthesis Models

Stellar population synthesis (SPS) models can be used to place constraints on  $\Upsilon_d$ . The combination of optical and in-

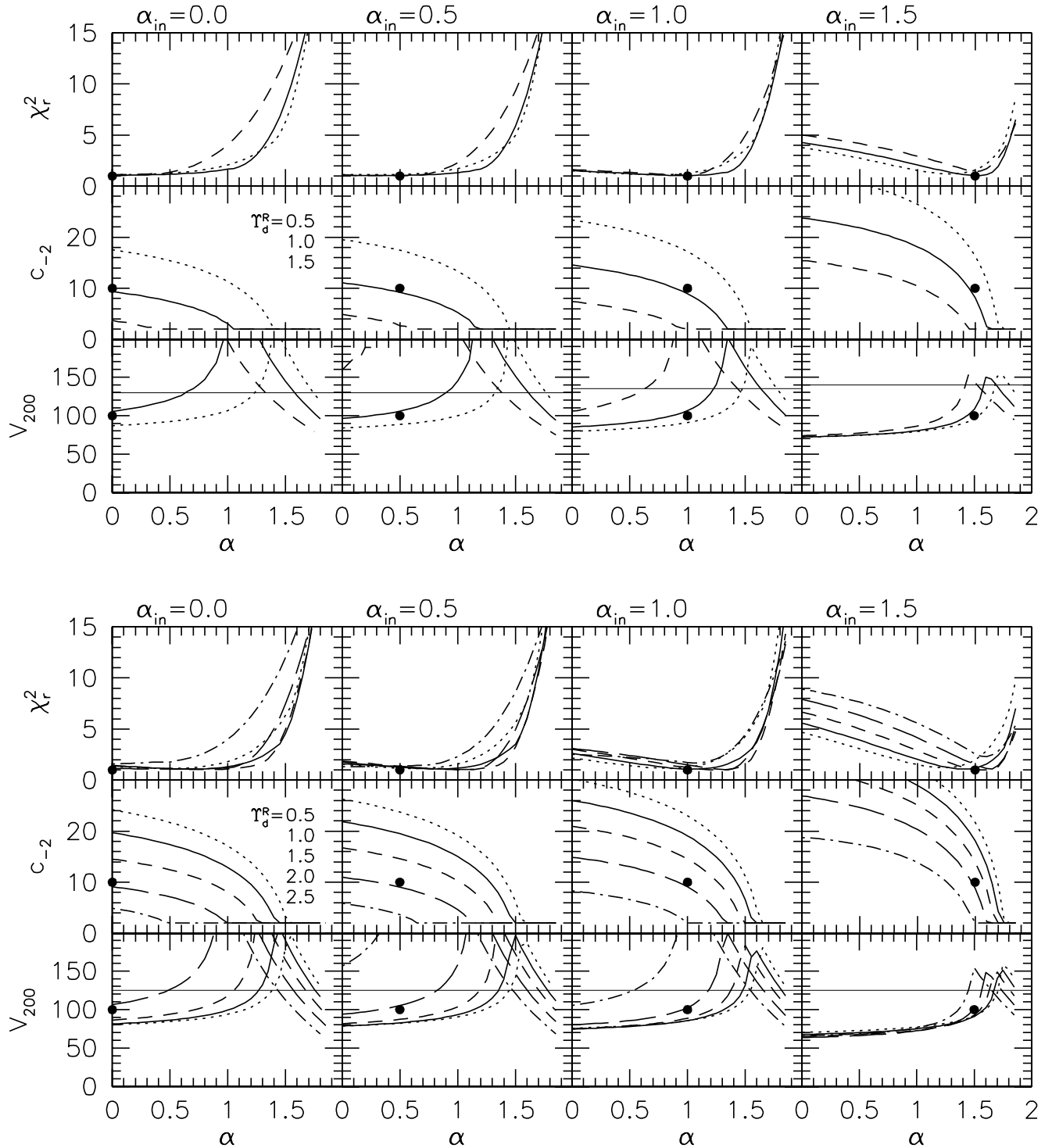


FIG. 6.— Best-fitting halo parameters and  $\chi_r^2$  for mock rotation curves vs.  $\alpha$ . All input models have adiabatically contracted (AC) halos with  $c_{-2} = 10$ ,  $V_{200} = 100$ , and exponential disks with  $\mu_0^R = 20$  and  $\Upsilon_d^R = 1.0$ . The only difference is in the central density slope,  $\alpha$ . The input models are indicated by the filled circles and have  $\chi_r^2 = 1.0$ . The top panels show fits with AC, while the bottom panels show fits without. The different lines correspond to different fitted mass-to-light ratios as indicated. The horizontal line indicates the maximum “observed” circular velocity. Note that we have imposed  $c_{-2} \geq 2$ .

frared photometry, with SPS models, yields  $\Upsilon_d$  values accurate to  $\sim 40\%$  (Bell & de Jong 2001). The slope of  $\Upsilon_d$  versus color is fairly independent of the initial mass function (IMF) and star formation (SF) history. That slope is also smaller in the  $K$ -band than in the  $B$ -band, although the zero point of the color- $\Upsilon_d$  relation is itself very sensitive to the IMF. The calibration of the  $\Upsilon_d$ -color relation by Bell & de Jong (2001) relies on the assumption of some galaxies being close to maximal disks, and their values of  $\Upsilon_d$  are thus upper limits.

#### 4.2. Evidence for Sub-Maximal Disks

A conventional hypothesis to determine an upper limit to  $\Upsilon_d$  is that disks should be maximal<sup>5</sup> (Carignan & Freeman 1985; van Albada & Sancisi 1986). This approach works well in practice for most HSB galaxies, but dark matter is still needed to explain the outer rotation curves of HSB and LSB galaxies at almost all radii. The fact that maximum disks can match inner rotation curves of HSB galaxies is more telling about the degeneracies in mass modeling than the validity of the hypothesis itself (Broeils & Courteau 1997; Courteau & Rix 1999). Furthermore,  $H\alpha$  rotation curves alone can often be fitted by pure disk or pure halo models and thus lack any constraining power without the addition of an extended HI rotation curve (Buchhorn 1992; Broeils & Courteau 1997).

By contrast to the maximal disk hypothesis, a variety of methods, which are described below, suggest that on average HSB disks are sub-maximal with

$$(V_{\text{disk}}/V_{\text{tot}})_{2.2} \simeq 0.6. \quad (10)$$

Note that a galaxy with a sub-maximal disk at  $2.2R_d$  can still be baryon dominated at  $2.2R_d$  if there is a significant bulge component.

##### 4.2.1. TFR Residuals

Courteau & Rix (1999) have suggested that sub-maximal disks should be invoked to explain the surface brightness independence of the Tully-Fisher relation (TFR); they find that, on average, HSB galaxies have  $(V_{\text{disk}}/V_{\text{obs}})_{2.2} \lesssim 0.6 \pm 0.1$  (see also Courteau et al. 2005). Their argument only depends on the assumptions that the scatter in the TFR and the size-luminosity relation (SLR) is dominated by a dependence in  $R_d$  and that dark halos respond adiabatically to the formation of the disk.

##### 4.2.2. Velocity Dispersion Measurements

The peak circular velocity of an isolated exponential disk can be related to the vertical velocity dispersion<sup>6</sup> and the intrinsic thickness of the disk,  $z_0$ , via (Bottema 1993)

$$V_{\text{disk}}^{\text{max}} = 0.88 \langle V_z^2 \rangle_{R=0}^{1/2} \sqrt{\frac{R_d}{z_0}}. \quad (11)$$

The factor 0.88 applies to a disk of zero thickness; for a thicker disk the peak velocity will be lower.

In practice, these measurements are difficult since the scale height,  $z_0$ , and scale length,  $R_d$ , of the disk cannot be measured simultaneously and the vertical velocity dispersions are easiest to measure in face-on galaxies although the disk kinematics is hard to determine. The prospects for this method

<sup>5</sup> We adopt the definition of a maximal disk as one that supplies  $85 \pm 10\%$  of the total velocity at  $2.2R_d$  (Sackett 1997).

<sup>6</sup> The correction to the velocity dispersion of a disk embedded in a dark matter halo is usually negligible (Bottema 1993).

are improving with the ability to reliably determine the inclinations for low-inclination galaxies using integral field spectroscopy (Verheijen et al. 2004).

Bottema (1993) found, for stellar kinematic measurements in 12 spiral galaxies (with  $V_{\text{obs}}^{\text{max}} > 100 \text{ km s}^{-1}$ ), that more massive spirals have larger velocity dispersions with the correlation  $\langle V_z^2 \rangle_{R=0}^{1/2} = \langle V_R^2 \rangle_{R=R_d}^{1/2} = (0.30 \pm 0.06) V_{\text{obs}}^{\text{max}}$ . Substituting this into equation (11) and taking the intrinsic disk scale ratio  $R_d/z_0 = 4.2 \pm 1.5$  (Kregel et al. 2002) yields

$$V_{\text{disk}}^{\text{max}}/V_{\text{obs}}^{\text{max}} = 0.5 \pm 0.2. \quad (12)$$

By comparison, Bottema (1993) obtained a mean value of 0.63, using  $R_d/z_0 = 6$ .

#### 4.2.3. Gravitational Lensing

In some rare cases in which a quasar is lensed by a foreground galaxy and gravitational lensing can be used to place an extra constraint on the mass profile, the dynamical analysis strongly favors sub-maximal disks (Maller et al. 2000; Trott & Webster 2002).

#### 4.2.4. Bars and Spiral Structure

It is generally thought that dynamical friction between the bar and halo will slow down the pattern speed of the bar; thus, fast bars imply maximal disks (Weinberg 1985; Hernquist & Weinberg 1992; Debattista & Sellwood 2000). However, other authors claim that the efficiency of bar slow-down by dynamical friction has been overestimated (Valenzuela & Klypin 2003) and that the bar pattern speed is not a reliable indicator of disk-to-dark matter ratio (Athanasoula 2003). Current observational data favor fast bar pattern speeds; however, only a handful of galaxies have reliable measurements (e.g., Debattista & Williams 2004), and most observations are of SB0 spiral galaxies, whose large bulge components and red colors are consistent with being baryon dominated.

In terms of late-type spiral galaxies, Weiner et al. (2001) modeled the strong shocks and non-circular motions in the observed gas flow and find that a high  $\Upsilon_d$ , corresponding to 80%-95% of  $V_{\text{disk}}$ , and a fast-rotating bar are highly favored. On the other hand, modeling of the spiral arm structure of a few grand-design galaxies by Kranz et al. (2003) yields a wide range of  $V_{\text{disk}}/V_{\text{tot}}$ , from closely maximal to 0.6. It should be noted that both these methods are model dependent and that while the basic dynamics of bars and spiral structure are understood, there are issues that remain to be resolved.

Courteau et al. (2003) showed that barred and non-barred galaxies belong to the same TFR. Thus, if the argument by CR99 is correct, barred galaxies would, on average, harbor sub-maximal disks. Note that this is consistent with the above observations, if there is significant scatter in  $V_{\text{disk}}/V_{\text{tot}}$ , or if  $V_{\text{disk}}/V_{\text{tot}}$  increases with surface brightness.

#### 4.3. Constraints on $V_{200}$

As shown in Figure 6, the fitted  $V_{200}$  often exceeds the maximum rotation velocity of the galaxy; by restricting  $V_{200} \leq V_{\text{max}}$ , the parameter space is reduced. For observed galaxies we expect  $V_{\text{max}}^{\text{obs}} \geq V_{\text{max}}$  provided that the rotation curve flattens out or declines at large radii, as is typical for extended rotation curves of spiral galaxies (Casertano & van Gorkom 1991).

The combined analysis of galaxy-galaxy lensing from the Sloan Digital Sky Survey (SDSS) and the TFR led Seljak

TABLE 1  
 GALAXY PARAMETERS

Galaxy	$M_B$ (mag)	Band	$\mu_0^{R,c}$ (mag arcsec $^{-2}$ )	$R_d$ (kpc)	$D$ (Mpc)	$V_{\odot}$ (km s $^{-1}$ )	$i$ (deg)	$1/\cos(i)$	$V_{\max}$	$R_{H\alpha}$	$R_{HI}$	References
(1)	(2)	(3)	(4)	(5)	(6)	(7)	(8)	(9)	(10)	(11)	(12)	(13)
NGC 3109.....	-16.35	<i>B</i>	22.3	1.3	1.36 <sup>c</sup>	403	75 ± 5	3.86	67	2.1	5.0	1, 2, 1, 3
IC 2574.....	-16.77	<i>R</i>	23.0	2.3	4.0 <sup>b</sup>	57	75 ± 7	3.86	67	–	4.6	4, 2, 4, 5
UGC 2259.....	-17.03	<i>r</i>	21.7	1.6	10.3 <sup>h</sup>	583	41 ± 3	1.33	90	1.4	4.8	6, 7, 8, 7
NGC 5585.....	-17.50	<i>R</i>	21.1	1.9	8.7 <sup>b</sup>	305	53 ± 1	1.66	92	2.7	7.1	9, 10, 9, 11
NGC 2403.....	-19.50	<i>r</i>	20.4	1.8	3.22 <sup>c</sup>	131	60 ± 2	2.00	136	2.1	10.8	12, 7, 8, 13
NGC 3198.....	-19.90	<i>r</i>	21.0	3.7	13.8 <sup>c</sup>	663	72 ± 2	3.24	157	1.8	12.0	12, 14, 8, 13

REFERENCES. — (1): Jobin & Carignan (1990); (2): Blais-Ouellette et al. (2001); (3): Musella et al. (1997); (4): Martimbeau et al. (1994); (5): Karachentsev et al. (2002); (6): Carignan et al. (1988); (7): Blais-Ouellette et al. (2004); (8): Kent (1987); (9): Côté et al. (1991). (10): Blais-Ouellette et al. (1999); (11): Drozdovsky et al. (2000); (12): Begeman (1987); (13): Freedman et al. (2001); (14): Corradi et al. (1991);

NOTE. — Col. (1): Galaxy name. Col. (2): Absolute *B* magnitude (Blais-Ouellette 2000). Col. (3): Photometry band; where necessary we convert to Cousins *R* assuming  $B-R=0.9$  or  $r-R=0.35$  (Jorgensen 1994). Col. (4): Central surface brightness in *R* band from a fit to the surface brightness profile with a marked disk, corrected for inclination (Col. [8]) and Galactic extinction (Schlegel et al. 1998). Col. (5): Scale length of the disk, from a fit to the *R*-band surface brightness profile with a marked disk. Col. (6): Adopted distance, with distance indicators “c” for Cepheid, “b” for brightest stars, and “h” for Hubble distance ( $h=0.7$ ) corrected for Virgo-centric flow (150 km/s). Col. (7): Systemic velocity; see HI reference. Col. (8): Inclination; see HI reference. Col. (9): Conversion factor we use to correct our  $\Upsilon_d$  for inclination, assuming a thin disk with no extinction. Col. (10): Maximum rotation velocity; see HI reference. Col. (11): Radius out to which we use the  $H\alpha$  rotation curve (in  $R_d$ ). Col. (12): Radius out to which we use the HI rotation curve (in  $R_d$ ). Col. (13): References, in the following sequence: HI,  $H\alpha$ , photometry, D.

(2002) to postulate that the rotation velocity of early- and late-type  $\sim L^*$  galaxies decreases significantly from its peak value at the optical radius ( $3.2R_d$ ) to the virial radius  $R_{200}$ , with

$$V_{\text{obs}}^{\max}/V(R_{200}) \simeq 1.8, \quad (13)$$

and a  $2\sigma$  lower limit of 1.4. This implies that the rotation curve declines at large radii and is thus inconsistent with an isothermal profile ( $\rho \propto r^{-2}$ ), unless the velocity excess over  $V(R_{200})$  is due entirely to the stellar component, which is unlikely for late-type galaxies. This result is consistent with Prada et al. (2003), who find  $\rho \propto r^{-3}$  at large radii.

Combining this constraint with the above evidence for sub-maximal disks, we get the interesting result that the total velocity at the virial radius is approximately equal to the peak velocity of the disk,

$$V_{\text{disk}}^{\max} \simeq V(R_{200}) \simeq V_{200}. \quad (14)$$

#### 4.4. Halo Concentration Parameter

Cosmological simulations suggest a correlation between  $c_{-2}$  and  $V_{\text{vir}}$ , such that more massive halos have lower concentrations (e.g., Bullock et al. 2001; Eke et al. 2001; Wechsler et al. 2002; Zhao et al. 2003). This is because halos with smaller masses collapse earlier, when the universe has a higher mean density. In the standard  $\Lambda$  CDM cosmology ( $\sigma_8 = 1.0, \Omega_M = 0.3$ ) for  $V_{200} = 100 \text{ km s}^{-1}$  the mean  $c_{-2} \simeq 12$ , but with a significant scatter of  $\Delta \log c_{-2} = 0.14$  (Wechsler et al. 2002). The mean  $c_{-2}$  is roughly proportional to  $\sigma_8$  and is also weakly dependent on  $\Omega_M$  such that lower  $\Omega_M$  gives lower  $c_{-2}$ . Given the current observational uncertainties in these parameters, the mean  $c_{-2}$  could easily be lowered by 25%. In the model of Bullock et al. (2001) for  $40 < V_{200} < 160$ , the  $2\sigma$  range in concentration is  $6 \lesssim c_{-2} \lesssim 30$ .

## 5. DATA

We now apply these constraints to a test sample of disk galaxies from Blais-Ouellette (2000). This sample is one of the few with rotation curves derived from both two-dimensional  $H\alpha$  and HI velocity fields. The  $H\alpha$  data are needed to probe the inner rising part of the rotation curve,

where resolution effects often limit the reliability of HI data. However, HI rotation curves are still needed to probe the outer part of the rotation curve (typically extending to twice the optical radius) and are essential to constrain the halo mass. The full Blais-Ouellette sample contains 10 galaxies, with a wide range of luminosities and surface brightnesses. We restrict our analysis to six of these galaxies that do not have significant bulges. Accurately decomposing the disk and bulge components and determining radial  $\Upsilon_d$  gradients requires near-IR imaging (e.g. *K* band) and optical color profiles. We will return to these issues in a forthcoming paper. Table 1 gives the optical and kinematic parameters of the sample galaxies, as well as references for the data sources. While this sample is by no means complete, it provides a representative selection of LSB and HSB “bulge-less” disk galaxies against which we can test our constraints.

#### 5.1. Rotation curve errors

Ideally, the rotation curve errors would be normally distributed and indicate the uncertainty in the circular velocity at a given radius. In practice, the errors are often defined in some ad hoc fashion, such as assigning a constant value to each velocity bin, and cannot be used to place confidence levels on fitted model parameters. We assume that the observed rotation velocity is equal to the circular velocity and therefore that non-circular motions (e.g., bars, streaming motions, pressure support) are not significant.

Blais-Ouellette (2000) computes errors on the  $H\alpha$  rotation curves using  $\sigma/\sqrt{N}$  in each ring of a tilted ring fit to the velocity field. By contrast, the errors on the HI rotation curves in our sample are computed using the velocity difference between the approaching and receding sides of the galaxy. To be consistent, we re-compute the errors on the  $H\alpha$  rotation curves by taking the maximum of  $\sigma/\sqrt{N}$  and the velocity difference between the two sides weighted by the number of points on each side. We also impose a minimum error of  $2 \text{ km s}^{-1}$  (to be consistent with the HI observations), although the actual uncertainty is probably larger. We investigate the effect of a larger minimum error value in §8.



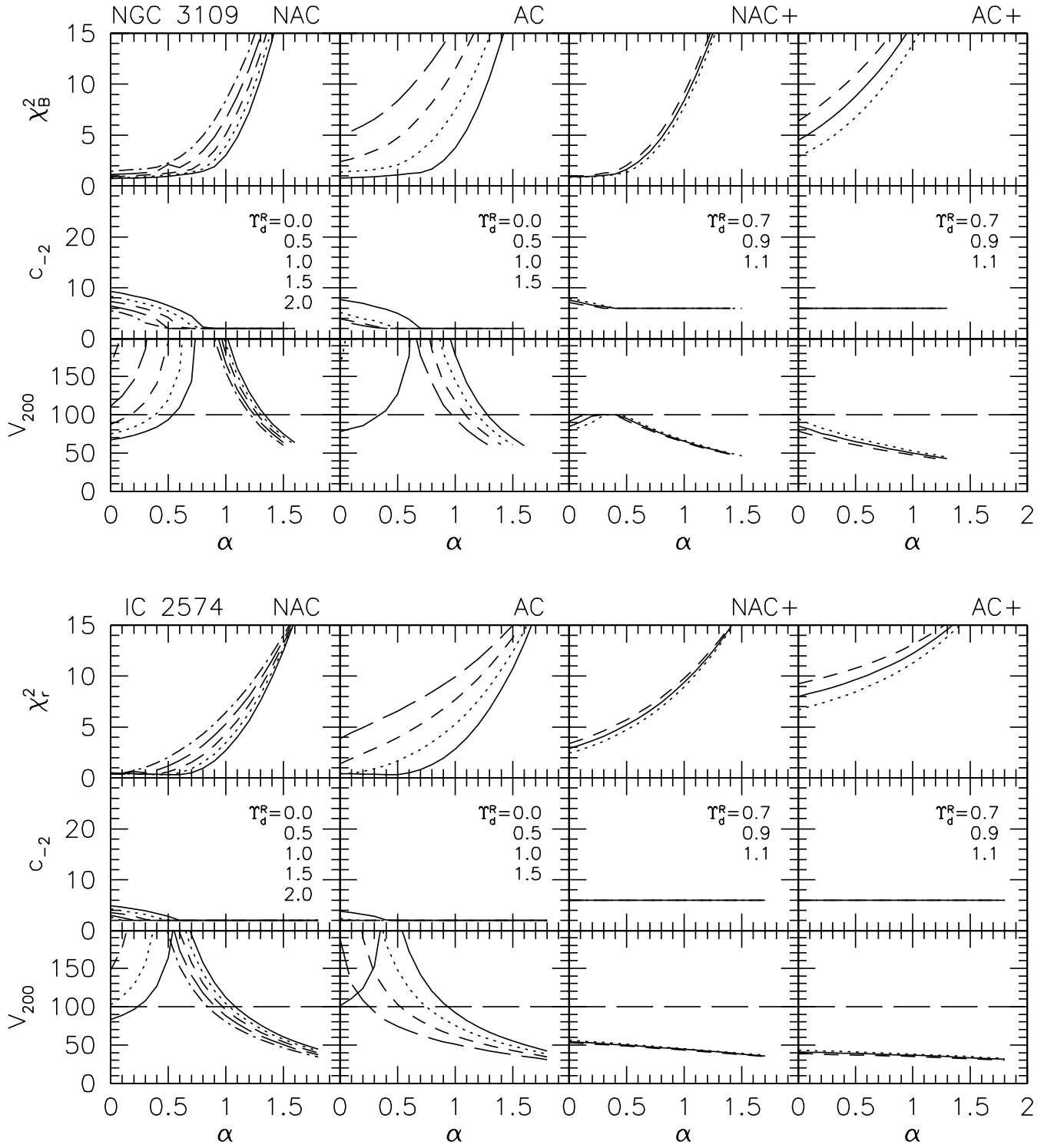


FIG. 7.— Best-fitting halo parameters and  $\chi_r^2$  vs.  $\alpha$  for a range of  $\Upsilon_d^R$  (as specified in the figures). We show fits with (AC) and without (NAC) adiabatic contraction and with (+) and without constraints on  $\Upsilon_d^R$ ,  $c_{-2}$ , and  $V_{200}$ . The dashed horizontal line indicates the constraint on  $V_{200}$ , from the maximum observed velocity; for NGC 2403 and NGC 3198 we also show  $V_{\max}/1.4$  and  $V_{\max}/1.8$ . For NGC 3109 and IC 2574 the rotation curves are still rising at the last measured point; here we set  $V_{200} < 100$ .

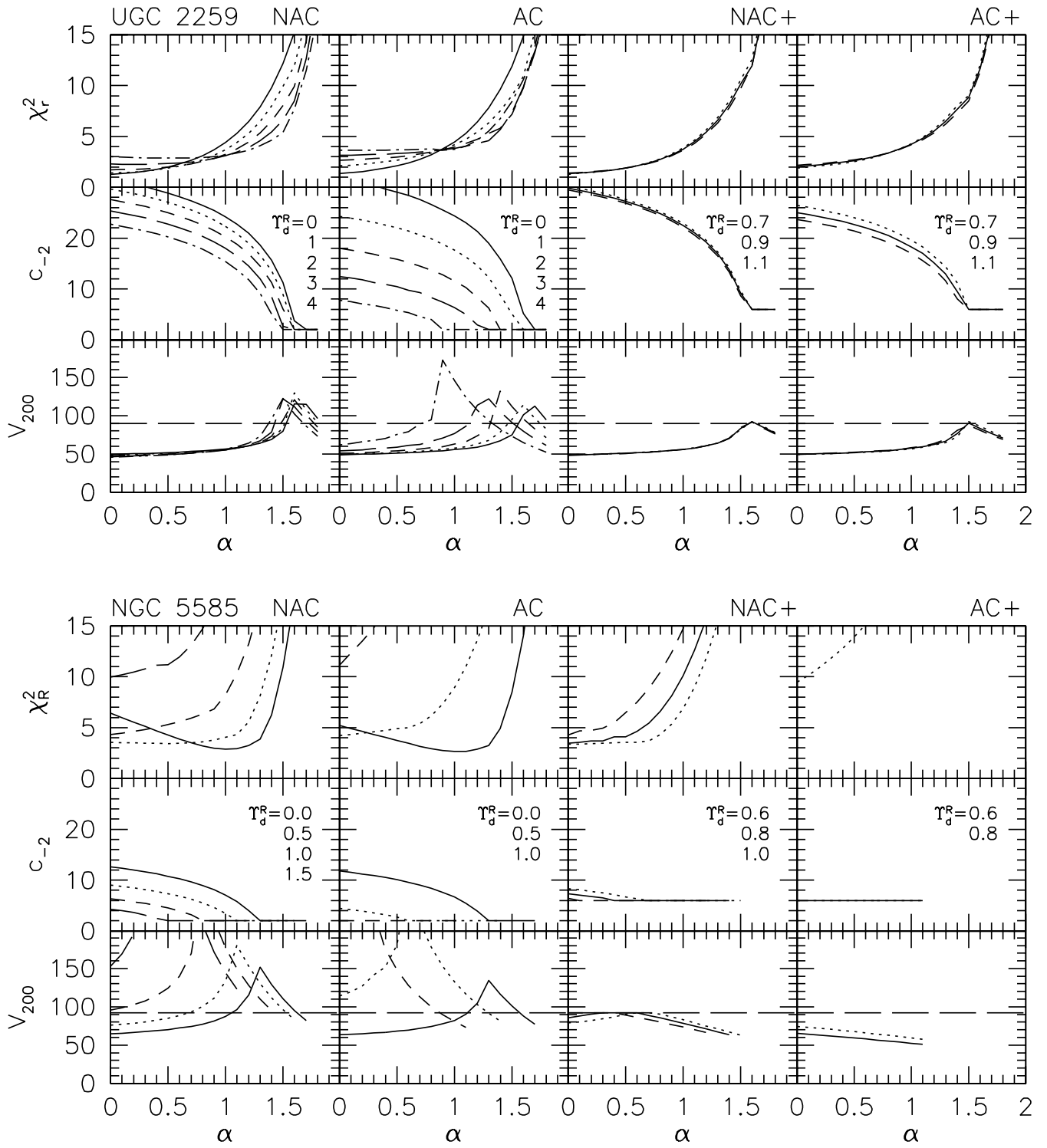


FIG. 7.— Continued.

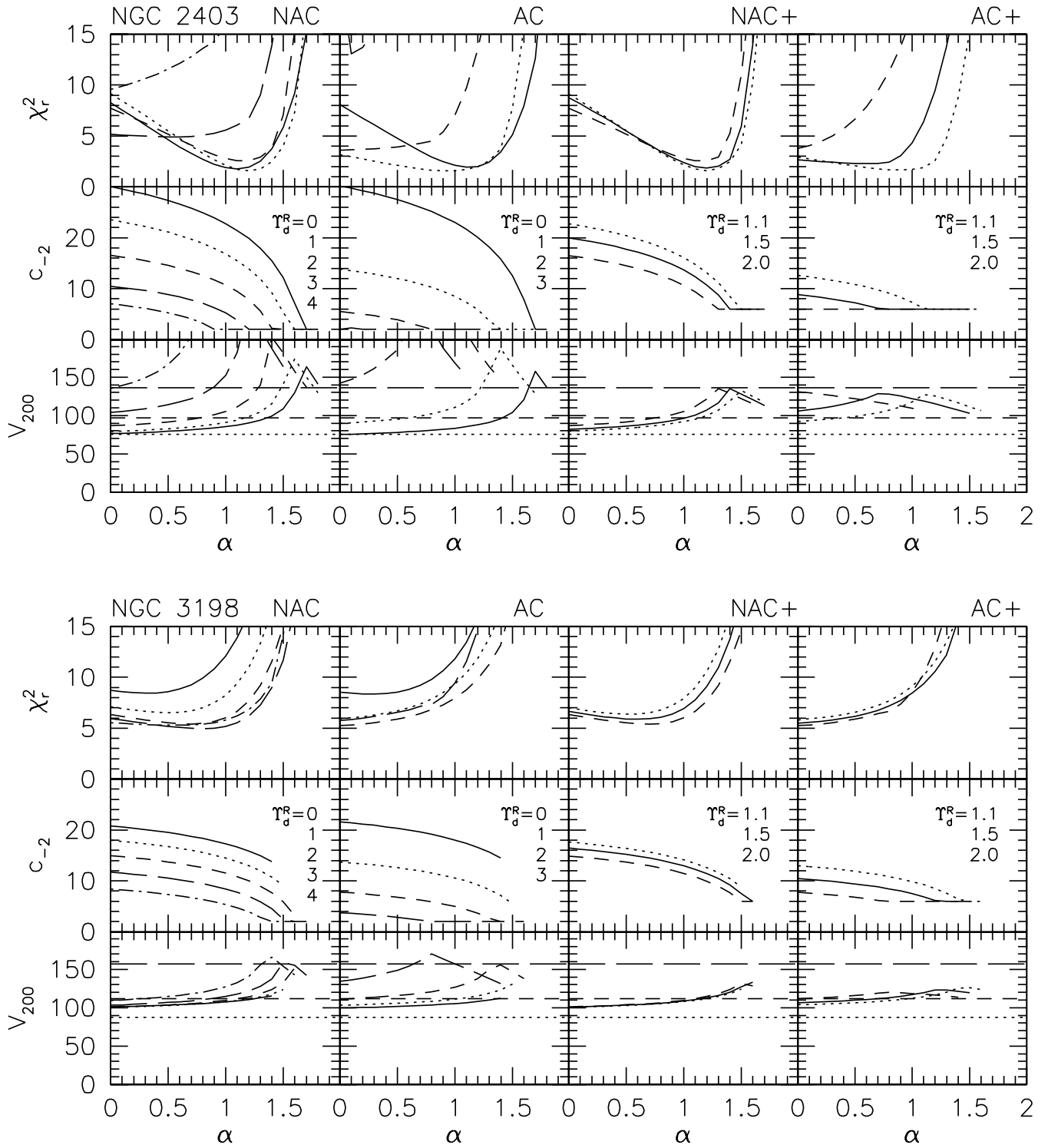
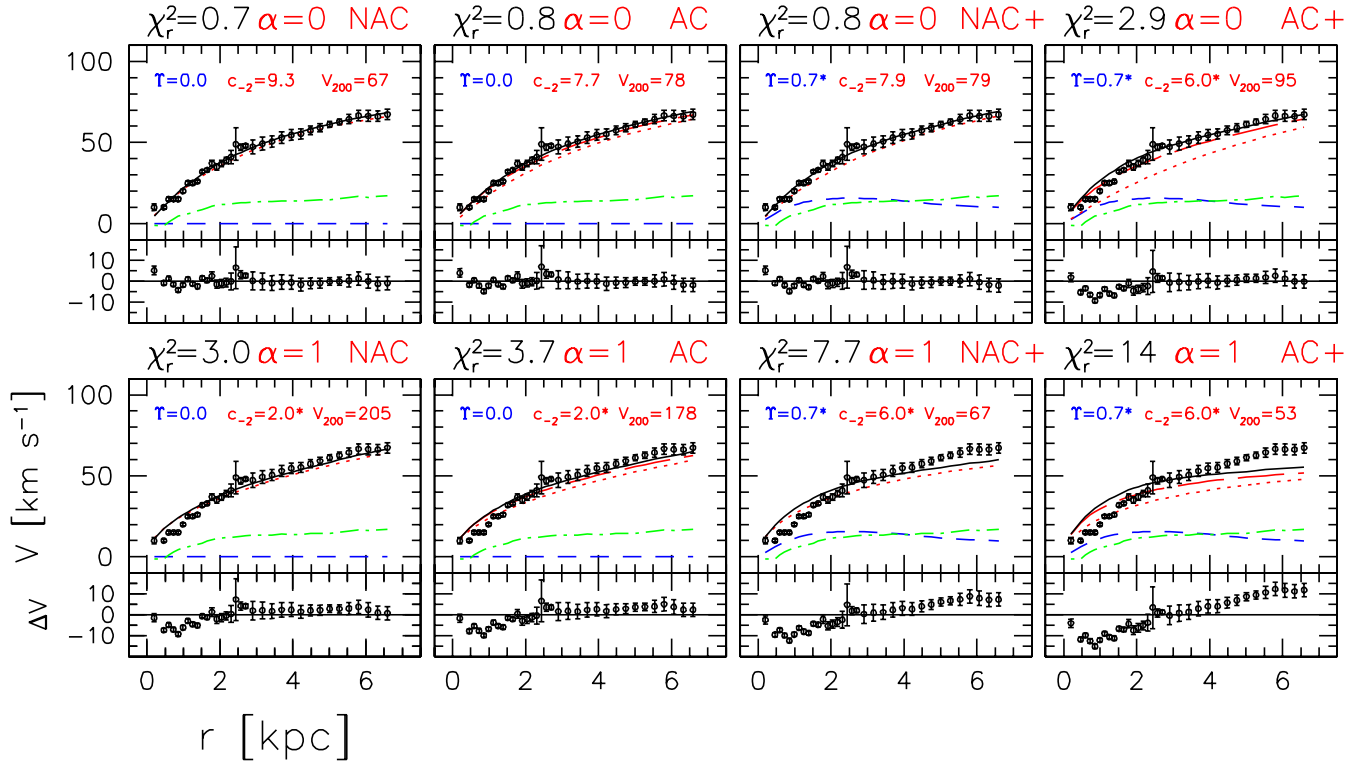


FIG. 7.— Continued.

## NGC 3109



## IC 2574

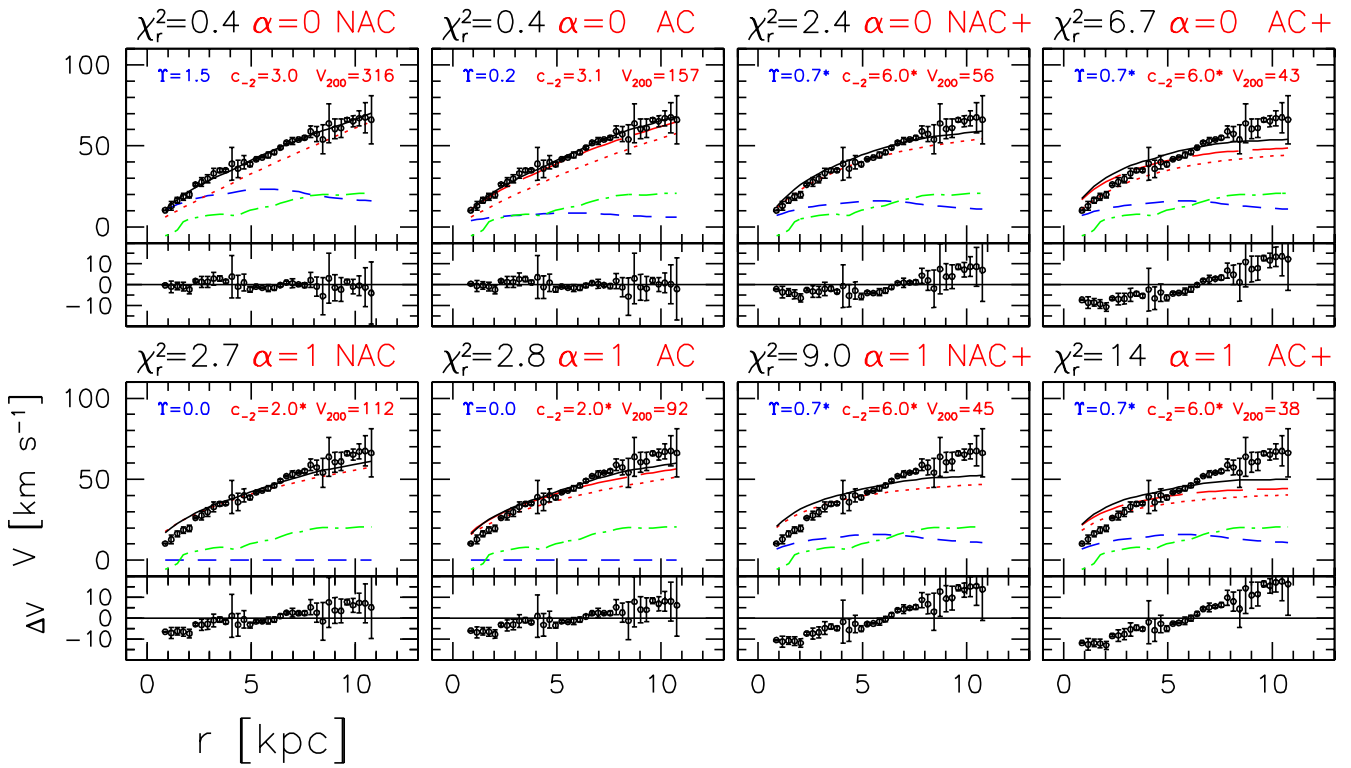
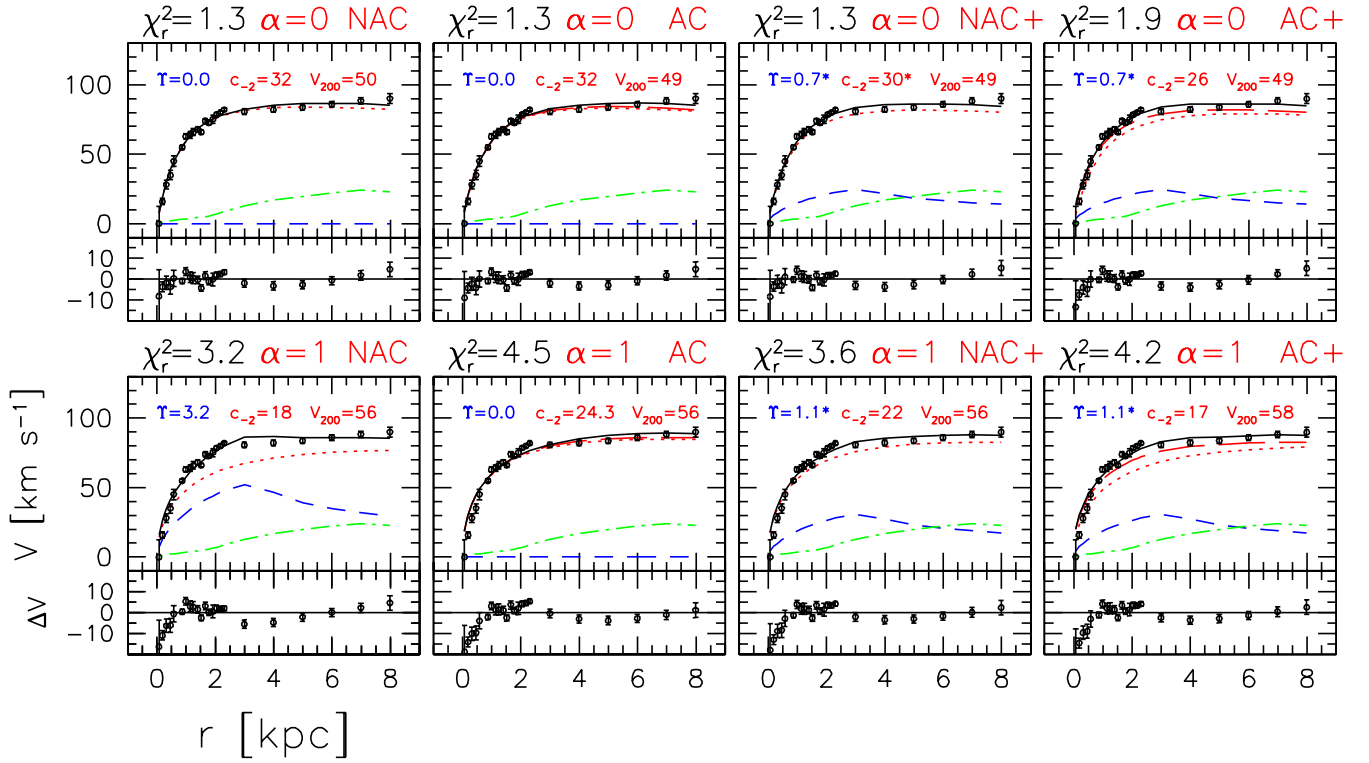


FIG. 8.— Sample rotation curve decompositions for all six galaxies. Shown are best fits (minimum  $\chi^2$ ) for  $\alpha = 0$  and  $\alpha = 1$ , with (AC) and without (NAC) adiabatic contraction and with (+) and without constraints on  $\Upsilon_{\text{d}}^R$ ,  $c_{-2}$ , and  $v_{200}$ . The total model rotation curves are given by the solid black lines; each model consists of three components: stellar disk (blue dashed line), gaseous disk (green dot-dashed line), and halo before/without AC (red dotted line) and after AC (red long-dashed line).

UGC 2259



NGC 5585

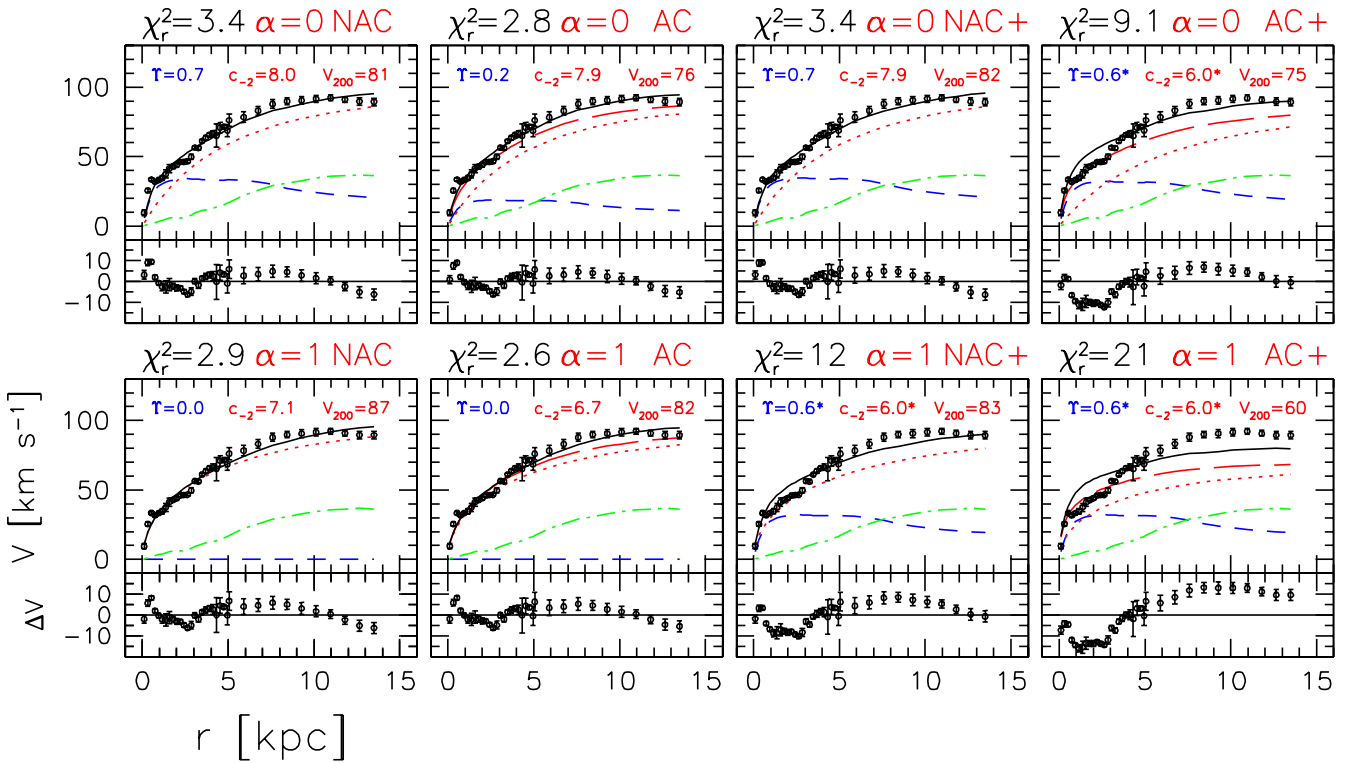


FIG. 8.— Continued.

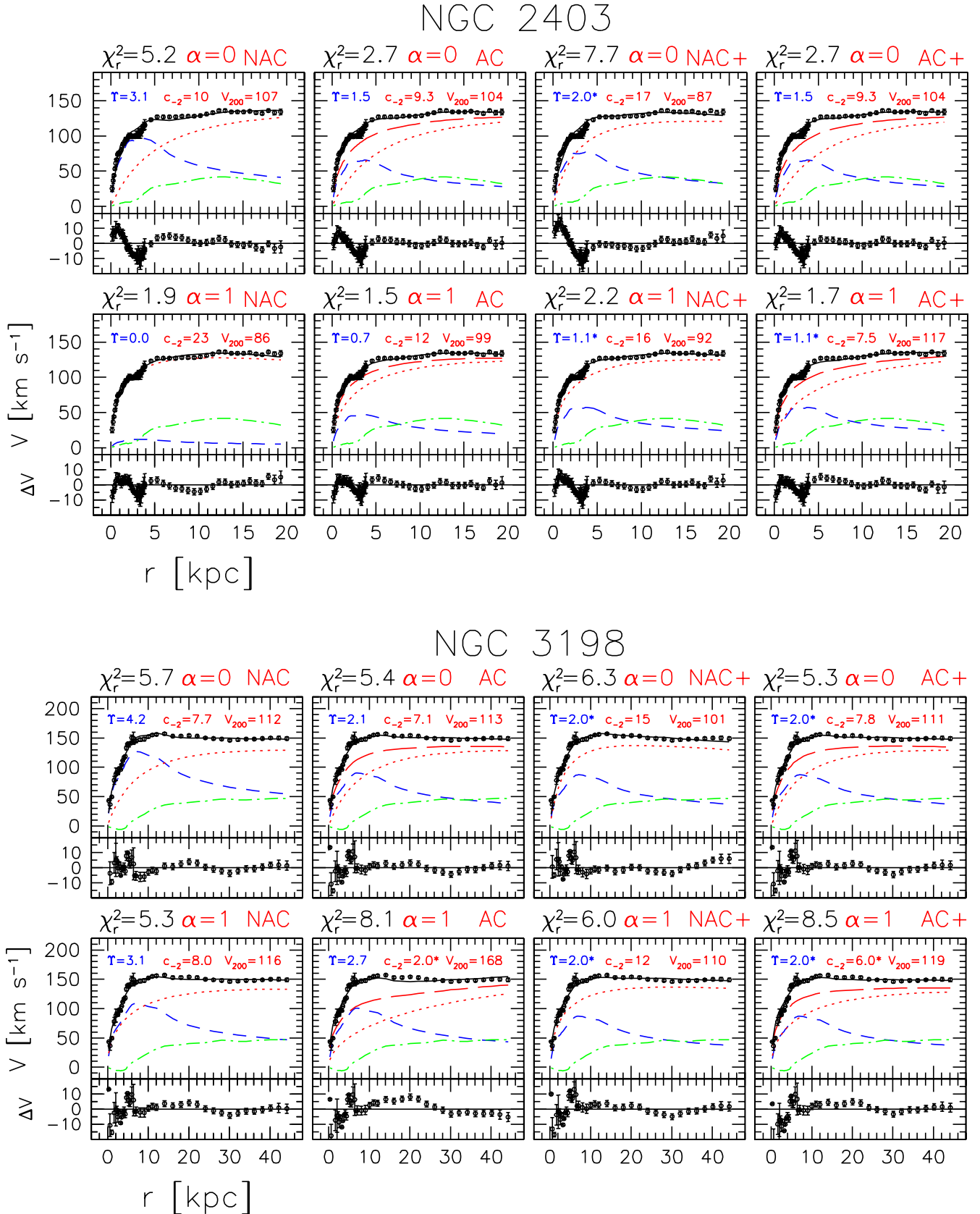


FIG. 8.— Continued.

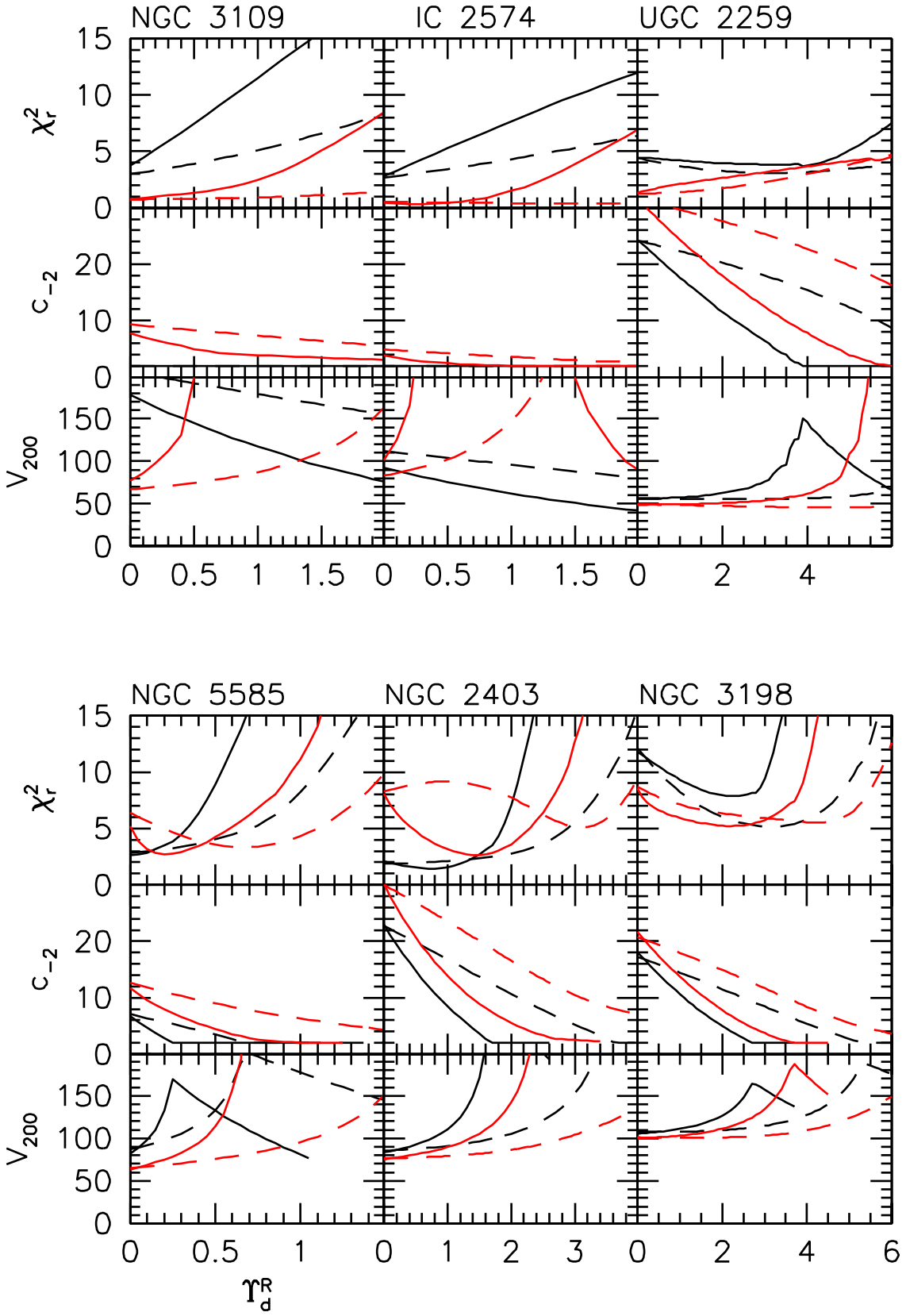


FIG. 9.— Effect on best-fit parameters of adiabatic contraction for halos with  $\alpha = 0$  (red) and  $\alpha = 1$  (black). Dashed lines show fits without AC, while solid lines show fits with AC.

### 5.2. Photometry uncertainties

In principle, observed surface brightness profiles should be corrected for projection and extinction effects to bring the profiles to their intrinsic face-on values. These have opposite effects on the surface brightness profile (the former leads to an over-estimate of the surface brightness, while the latter causes it to be under-estimated). In practice, these corrections are fraught with significant uncertainties, especially for extinction correction. For simplicity we only correct for inclination assuming that the disk is optically thin and of zero thickness. Thus, the observed surface density will be a factor of  $1/\cos(i)$  greater than the face-on case, where  $i$  is the inclination angle. The adopted inclination angles are given in Table 1. We correct for Galactic extinction using the reddening values of Schlegel et al. (1998). The effect of internal dust extinction is to reduce the observed surface brightness from its intrinsic (stellar) value and is expected to have some radial dependence. Thus, the simple dust-free model that we adopt, all other variables being equal, gives an *upper limit* to the  $\Upsilon_d^R$ .

## 6. ROTATION CURVE FITS

As a result of certain covariances between model parameters, we fit for  $c_{-2}$  and  $V_{200}$  on a grid of  $\Upsilon_d^R$  and  $\alpha$  to prevent our fitting routine from getting trapped in local minima. The results of these fits are shown in Figure 7, where we plot the reduced  $\chi^2$  and best-fit  $c_{-2}$  and  $V_{200}$  against  $\alpha$  for a range of  $\Upsilon_d^R$  from zero to maximum disks. Examples of rotation curve decompositions for  $\alpha = 0$  and  $\alpha = 1$  halos are shown in Fig. 8. Clearly, without constraints the models are highly degenerate, with acceptable fits being possible covering a wide, ill-constrained range of  $\alpha$  and  $\Upsilon_d^R$ .

### 6.1. Effect of adiabatic contraction

In Figure 9 we plot the  $\chi_r^2$  and best fit  $c_{-2}$  and  $V_{200}$  versus  $\Upsilon_d^R$ , for  $\alpha = 0$  and  $\alpha = 1$  halos. Adiabatic contraction causes the rotation velocity of the halo to rise, especially at small radii. Thus, to obtain a comparable circular velocity profile, the concentration of the pre-contracted halo must be lower. As  $\Upsilon_d^R$  increases, this effect becomes more significant and can substantially alter the halo parameters, even for sub-maximal disks. For close to maximum disks acceptable fits cannot be obtained without breaking the weak constraint:  $c_{-2} \geq 2$ . Even after exclusion of the high  $V_{\text{disk}}/V_{\text{tot}}$  solutions, the disk-halo and cusp-core degeneracies still remain. In general, the best-fit  $\chi_r^2$  values are lower with adiabatic contraction than without. In cases in which a maximum disk is the preferred fit without adiabatic contraction, the best-fit  $\Upsilon_d^R$  and  $\chi_r^2$  are both lower with adiabatic contraction.

### 6.2. Fits with constraints

*SPS models.*—Table 2 gives the observed or expected  $B-R$  colors and the predicted  $\Upsilon_d^R$  using the formula  $\log(\Upsilon_d^R) = -0.820 + 0.851(B-R)$  (Table 1, Bell & de Jong 2001). We find that the galaxy colors and the SPS-predicted  $\Upsilon_d^R$  values are significantly lower than the rotation curve-derived maximal disk values for five out of six galaxies, the exception being NGC 5585, although the latter is dark matter dominated at larger radii. In terms of velocities  $(V_{\text{disk}}/V_{\text{tot}})_{2.2} \lesssim 0.6$  for all six galaxies. As we have not included internal extinction effects, the intrinsic colors will be bluer and the resulting  $\Upsilon_d^R$

and disk velocity fractions will be lower. The maximal disk  $\Upsilon_d^R$  for NGC 5585 is inconsistent with  $\alpha \simeq 1$  halos and cannot be reconciled with any halo that is adiabatically contracted.

*Sub-maximal disks.*—NGC 3198 has a measured velocity dispersion,  $\langle V_z^2 \rangle_{R=0}^{1/2} = 40 \pm 0.7$  (Bottema 1993), implying  $(V_{\text{disk}}/V_{\text{obs}})_{\text{max}} = 0.43 \pm 0.15$ . For NGC 2403 we apply the sub-maximal disk constraint (Eq. 10). The associated  $\Upsilon_d^R$  are given in Table 2 and are consistent with the expected  $\Upsilon_d^R$  from SPS models. *These constraints rule out zero and maximal disks but do not break the disk-halo degeneracy for NGC 2403 and NGC 3198, even when the halos are adiabatically contracted.*

*The  $c_{-2} - V_{200}$  comparison.*—In Figure 10 we compare the fitted  $c_{-2}$  and  $V_{200}$  for  $\alpha = 1$  and  $\alpha = 0$  halo fits with the  $c_{-2} - V_{200}$  model of Bullock et al. (2001). This shows that as  $\Upsilon_d^R$  increases, the fitted  $c_{-2}$  decreases and  $V_{200}$  increases. For a given  $\Upsilon_d^R$ , fits with  $\alpha = 0$  have larger  $c_{-2}$  and lower  $V_{200}$  than fits with  $\alpha = 1$ , but the differences are not significant enough to distinguish between  $\alpha = 0$  and  $\alpha = 1$ . Fits with adiabatic contraction follow the same path in the  $c_{-2} - V_{200}$  space as those without, such that for a given  $\Upsilon_d^R$  the  $c_{-2}$  of the adiabatic contraction halos are lower. (Note that the  $c_{-2}$  and  $V_{200}$  values of the contracted halos are those of the *initial* pre-contracted halo.) For NGC 2403, NGC 3198, and UGC 2259 the  $\Upsilon_d^R$  values from SPS models fall within  $1\sigma$  of the mean  $c_{-2}$  for  $\alpha = 1$  halos, while for IC 2574, NGC 3109, and NGC 5585 the  $\Upsilon_d^R$  from SPS models require very low  $c_{-2}$ .

*Lensing-TF.*—This constraint (Eq. 14) corresponds to  $V_{200} = 76^{+21}$  and  $87^{+25}$   $\text{km s}^{-1}$  for NGC 2403 and NGC 3198, respectively. Note that there is no lower limit on  $V_{200}$ . From Fig. 7, we see that for NGC 2403 the lowest  $V_{200} = 75$   $\text{km s}^{-1}$ , while for NGC 3198 the lowest  $V_{200} = 100$   $\text{km s}^{-1}$ . These values occur when  $c_{-2}$  is highest, which corresponds to  $\alpha = 0$  and  $\Upsilon_d^R = 0$ . As  $\alpha$  and  $\Upsilon_d^R$  increase,  $c_{-2}$  decreases and  $V_{200}$  increases, so that the highest (and thus excluded) values of  $V_{200}$  occur for cuspy halos with close to maximal disks. Thus, this constraint favors low  $\alpha$  and  $\Upsilon_d^R$  fits.

*All constraints.*—Our full set of constraints consist of  $\Upsilon_d^R$  from SPS models,  $6 \leq c_{-2} \leq 30$ , and  $V_{200} \leq V_{\text{max}}$ . The rotation curves for NGC 3109 and IC 2574 are still rising at the last data point, so we adopt  $V_{\text{max}} = 100$ , consistent with other dwarf galaxies. In Table 3 we give the ranges in  $\alpha$  that are within 3.5 of the best-fit  $\chi_r^2$ . While we cannot place a statistical confidence on these ranges, they seem to encompass all of our acceptable fits. Clearly, even with the full set of constraints significant degeneracies remain, often with both  $\alpha \simeq 0$  and  $\alpha \simeq 1$  halos providing reasonable fits. The differences between fits with and without adiabatic contraction can be substantial. Given that other evolutionary processes exist and are not clearly understood, there remains significant uncertainty in determining  $\alpha$ .

## 7. OTHER UNCERTAINTIES IN MASS MODELS

We now discuss the sensitivity of our results to several parameters that have so far been kept fixed. These include the minimum rotation curve error values,  $dV_{\text{min}}$ ; the distance,  $D$ ; the disk thickness,  $q_d$ ; and the halo flattening,  $q_h$ . Results for the tests we perform below are shown in Fig. 11 for  $\alpha = 0$  and  $\alpha = 1$  halos without adiabatic contraction. The results are similar with adiabatic contraction, but the range in  $\Upsilon_d^R$  is lower.

*Minimum rotation curve error values.*—We use minimum error values for each velocity measurement at a given radius



TABLE 2  
 MASS-TO-LIGHT RATIOS FROM CONSTRAINTS

Galaxy (1)	$\Upsilon_{d,\max}^R$ (2)	$(B-R)_{\max}$ (3)	$(B-R)_{\text{obs}}$ (4)	$\Upsilon_{d,\text{sps}}^R$ (5)	$\Upsilon_{d,\text{sub}}^R$ (6)	$(V_{\text{disk}}/V_{\text{tot}})_{2.2}^+$ (7)	$(V_{\text{disk}}/V_{\text{tot}})_{\max}^+$ (8)
NGC 3109.....	1.5	1.17	$0.9 \pm 0.1^a$	$0.88^{+0.19}_{-0.15}$	-	0.33	0.23
IC 2574.....	1.5	1.17	$0.90^b$	0.88	-	0.41	0.24
UGC 2259.....	8.0	2.02	$0.9 \pm 0.1^a$	$0.88^{+0.19}_{-0.15}$	-	0.38	0.33
NGC 5585.....	0.7	0.78	$0.86^c$	0.82	-	0.47	0.35
NGC 2403.....	3.1	1.54	$1.17 \pm 0.15^d$	$1.5^{+0.5}_{-0.4}$	$1.1^{+1.1}_{-0.7}$	0.50	0.42
NGC 3198.....	4.2	1.70	$1.17 \pm 0.15^d$	$1.5^{+0.5}_{-0.4}$	$1.1^{+0.8}_{-0.6}$	0.59	0.56

NOTE. — Col. (1): Galaxy name. Col. (2): Maximum disk  $\Upsilon_d^R$  from fits including a dark halo; for disk only models the  $\Upsilon_d^R$  are up to  $\sim 25\%$  higher. Col. (3): Predicted  $B-R$  color for the  $\Upsilon_d^R$  in col. (2) based on SPS models from Bell & de Jong (2001). Col. (4): Observed or expected  $B-R$  color. Col. (5) predicted  $\Upsilon_d^R$  for the  $B-R$  color given in col. (4) using Bell & de Jong (2001); Col. (6)  $\Upsilon_d^R$  based on the sub-maximal disk constraints from Bottema (1993); Col. (7) ratio of disk velocity to total observed rotation velocity at 2.2 disk scale lengths for the best fit  $\Upsilon_d^R$  with constraints. Col. (8) ratio of maximum disk to maximum observed rotation velocities for the  $\Upsilon_d^R$  from Col. (7).

<sup>a</sup>Expected  $B-R$  color for dwarf disk galaxies (e.g. van den Bosch & Swaters [2001] find  $\langle B-R \rangle = 0.87 \pm 0.09$  for six late-type dwarf galaxies).

<sup>b</sup>Martimbeau et al. (1994) corrected for Galactic reddening.

<sup>c</sup>Côté et al. (1991) corrected for Galactic reddening.

<sup>d</sup>Mean  $B-R$  color of 40 late-type HSB disk galaxies from MacArthur et al. (2003).

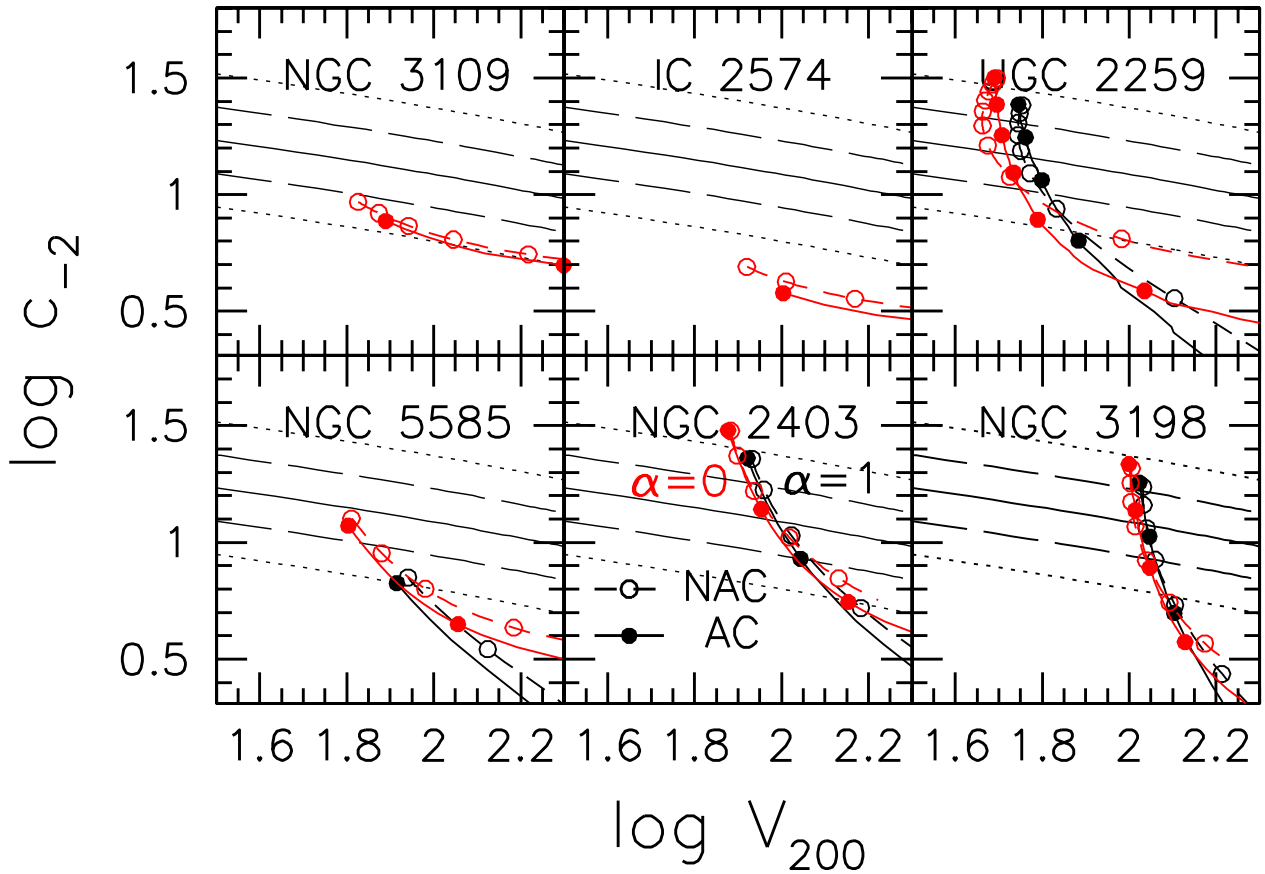


FIG. 10.— Comparison between our fitted  $c_{-2}$  and  $V_{200}$  against the model from Bullock et al. (2001). The mean is given by the solid line, while the 1 and 2  $\sigma$  deviations are given by the long-dashed and dotted lines, respectively. Fits with  $\alpha = 0$  are in black, while fits with  $\alpha = 1$  are in red. Fits with adiabatic contraction (AC) are given by filled circles and solid lines, while fits without AC (NAC) are given by open circles and dotted lines. For NGC 3109, IC 2574, and NGC 5585 the symbols are at  $\Upsilon_d^R$  intervals of 0.5, while for UGC 2259, NGC 2403, and NGC 3198 the interval is 1.0.

TABLE 3  
RANGE AND BEST-FIT VALUES OF  $\alpha$ .

Galaxy (1)	$\alpha_{NAC}$ (2)	$\alpha_{AC}$ (3)	$\alpha_{NAC+}$ (4)	$\alpha_{AC+}$ (5)
NGC 3109.....	0.0 <sup>1.1</sup> <sub>0.0</sub>	0.0 <sup>1.1</sup> <sub>0.0</sub>	0.0 <sup>0.8</sup> <sub>0.0</sub>	0.0 <sup>0.3</sup> <sub>0.0</sub>
IC 2574.....	0.0 <sup>1.1</sup> <sub>0.0</sub>	0.0 <sup>1.1</sup> <sub>0.0</sub>	0.0 <sup>0.4</sup> <sub>0.0</sub>	—
UGC 2259.....	0.0 <sup>1.5</sup> <sub>0.0</sub>	0.0 <sup>1.3</sup> <sub>0.0</sub>	0.0 <sup>1.1</sup> <sub>0.0</sub>	0.0 <sup>1.1</sup> <sub>0.0</sub>
NGC 5585.....	1.0 <sup>1.4</sup> <sub>0.0</sub>	1.0 <sup>1.4</sup> <sub>0.0</sub>	0.5 <sup>0.9</sup> <sub>0.0</sub>	—
NGC 2403.....	1.2 <sup>1.3</sup> <sub>0.0</sub>	0.9 <sup>1.3</sup> <sub>0.0</sub>	1.2 <sup>1.3</sup> <sub>0.0</sub>	1.0 <sup>1.3</sup> <sub>0.0</sub>
NGC 3198.....	0.9 <sup>1.4</sup> <sub>0.0</sub>	0.0 <sup>1.1</sup> <sub>0.0</sub>	0.8 <sup>1.3</sup> <sub>0.0</sub>	0.0 <sup>1.0</sup> <sub>0.0</sub>

NOTE. — Col. (1): galaxy name. Col. (2): best fit and upper and lower limits based on a  $\Delta\chi_r^2 = 3.5$  for fits without adiabatic contraction (AC) or constraints (+). Col. (3): Same as col. (2), but for fits with AC. Col. (4): Same as col. (4), but for fits with constraints. Col. (5): Same as col. (2), but for fits with AC and constraints.

of 2, 3, and 4  $\text{km s}^{-1}$ . Larger error values have the effect of lowering the  $\chi_r^2$  and make it harder to distinguish between models.

*Distance.*—We show the effect of a 30% distance error, in order to account for uncertainties in distance estimation such as peculiar velocities. The mass of the stars and gas is proportional to distance, so for larger distances and a given  $V_{\text{disk}} \Upsilon_d^R$  is lower.

*Disk thickness.*—We consider the values of  $q_0 = 0$  for a thin disk, the commonly-used  $q_0 = 1/6$ , and  $q_0 = 0.25$ . The effect of a thick disk is to smooth out the features of the surface brightness profile and lower the amplitude of the rotation curve (Fig. 12). This results in a higher maximum disk  $\Upsilon_d^R$  but does not significantly alter the relative goodness of fit between  $\alpha = 0$  and  $\alpha = 1$  halos.

*Halo flattening.*—We compute fits for oblate halos with  $q = 0.25$  and  $q = 0.5$  and a prolate halo with  $q = 1.5$ . The effect of halo flattening on  $\chi_r^2$  is very small, and is only noticeable for low  $\Upsilon_d^R$  fits because the halo parameters adjust; as  $q$  decreases,  $c_{-2}$  decreases and  $V_{200}$  stays roughly constant. Because we define  $R_{200}$  to be independent of  $q$ , then for a given  $r_{-2}$ ,  $V_{200}$  increases as  $q$  decreases. Therefore, if  $V_{200}$  is constant,  $c_{-2}$  will decrease as  $q$  decreases. Thus, although halo flattening does not alter the  $\chi_r^2$ , it contributes an additional  $\sim 20\%$  uncertainty to  $c_{-2}$ .

## 8. SUMMARY

There has been much debate recently over the shape of galaxy density profiles, especially regarding the center of dwarf and LSB galaxies that are believed to be dark matter dominated. However, a large number of systematic effects such as slit position error, poorly sampled velocity fields, and non-circular motions thwart the straightforward interpretation of observed rotation curves as circular velocity profiles.

Even if the circular velocity profile is measured perfectly, the determination of  $\alpha$  is complicated by the degeneracies inherent to the mass modeling exercise. The most cited degeneracy is that of the unknown value of the stellar mass-to-light ratio,  $\Upsilon_d$ ; strong covariances with the halo concentration and density profile slope prevent a definitive determination of  $\Upsilon_d$ . Even if  $\Upsilon_d$  were known, degeneracies that exist between the halo parameters might also prevent a unique determination of  $\alpha$ .

Independent constraints may help in breaking these degeneracies. We have considered such constraints with six disk galaxies that have  $\text{H}\alpha$  and HI rotation curves and  $R$ -

band imaging. The  $\text{H}\alpha$  rotation curves are derived from two-dimensional Fabry-Perot velocity fields (Blais-Ouellette 2000; Corradi et al. 1991) and as such are not affected by most of the systematic caveats raised by Swaters et al. (2003a) on the context of long-slit spectroscopy and low-resolution radio-synthesis mapping, such as slit position error and beam smearing. However, we cannot exclude the possibility of non-circular motion effects in these rotation curves.

The advantages of two-dimensional  $\text{H}\alpha$  velocity fields over long-slit spectra are demonstrated with UGC 2259, also studied by Swaters et al. (2003a). Sampling more of the velocity field yields a scatter in the rotation curve data of Blais-Ouellette et al. (2004) that is significantly smaller than that of the long-slit spectrum of the same object by Swaters et al. (2003a). These authors find  $\alpha = 0.86 \pm 0.18$  for a minimum disk, and their plot of  $\chi^2$  versus  $\alpha$  is mostly flat for  $0 < \alpha < 1$  for all  $\Upsilon_d$ . By contrast, we find the best fit  $\alpha = 0$  for all  $\Upsilon_d^R$ , and the  $\chi_r^2$  increases with  $\alpha$ . It should be noted that  $\alpha = 1$  halo fits for UGC 2259 deviate most strongly in the central 0.5 kpc ( $\simeq 0.01R_{200}$ ) where systematic effects on the rotation curve are most significant.

For galaxies with appreciable baryonic components, the formation of the disk may have altered the initial dark matter density profile. To first order the halo contracts, but other mechanisms such as stellar feedback and stellar bars may result in less concentrated halos. To encompass the full range, we run fits with and without adiabatic contraction. Adiabatic contraction has the effect of turning cores into cusps, even for relatively low mass disks. The effect of adiabatic contraction on the circular velocity and density slope increases for larger  $\Upsilon_d^R$ , lower  $c_{-2}$ , and lower  $\alpha$ . Obviously, maximal disks are inconsistent with adiabatic contraction.

Applying the SPS model of Bell & de Jong (2001) to the expected or observed  $B-R$  colors for these galaxies implies that all galaxies are sub-maximal at  $2.2R_d$ . This is in agreement with other independent techniques that suggest that HSB disk galaxies have, on average, sub-maximal disks with  $V_{\text{disk}}^{\text{max}} \simeq 0.6V_{\text{obs}}^{\text{max}}$  (e.g., Bottema 1993, 1997; Courteau & Rix 1999; Trott & Webster 2002; Courteau et al. 2005).

In the model from  $N$ -body simulations of Bullock et al. (2001) for halos with  $50 \lesssim V_{200} \lesssim 160 \text{ km s}^{-1}$ , the  $2-\sigma$  range in concentrations is  $6 \lesssim c_{-2} \lesssim 30$ . By defining the concentration parameter as  $c_{-2} = r_{200}/r_{-2}$ , where  $r_{-2}$  is the radius where the density slope of the halo is  $-2$ , these constraints can be applied to halos of arbitrary  $\alpha$ . All fits have  $c_{-2} \lesssim 30$ , but often fits with  $\alpha \gtrsim 1$  have  $c_{-2} \lesssim 6$ . Applying this constraint to mass models thus lowers the range of acceptable  $\alpha$ . As a further constraint, we impose  $V_{200} \leq V_{\text{max}}$ ; this constraint does not significantly affect the best fits, but it does help to eliminate bad ones. If we impose the stronger constraint  $V_{200} \leq V_{\text{max}}/1.4$  for bright galaxies (NGC 2403 and NGC 3198), values of  $\alpha \gtrsim 1$  are disfavored.

Without constraints NGC 3109 and IC 2574 strongly favor  $\alpha \simeq 0$  and low  $\Upsilon_d^R$ , although both of these galaxies are not ideally suited for mass modeling studies (NGC 3109 has an uncertain inclination angle, and IC 2574 has a disrupted velocity field). The remaining four galaxies are consistent with a wide range of central density slopes  $0 \lesssim \alpha \lesssim 1.4$  and mass-to-light ratios,  $\Upsilon_d^R$ . Applying our full set of constraints reduces the range of acceptable  $\alpha$ , but taking fits with and without adiabatic contraction as two extremes, there still remains a wide range of acceptable  $\alpha$ , and only for NGC 5585 can we strongly distinguish between  $\alpha \simeq 0$  and  $\alpha \simeq 1$  (in this case,

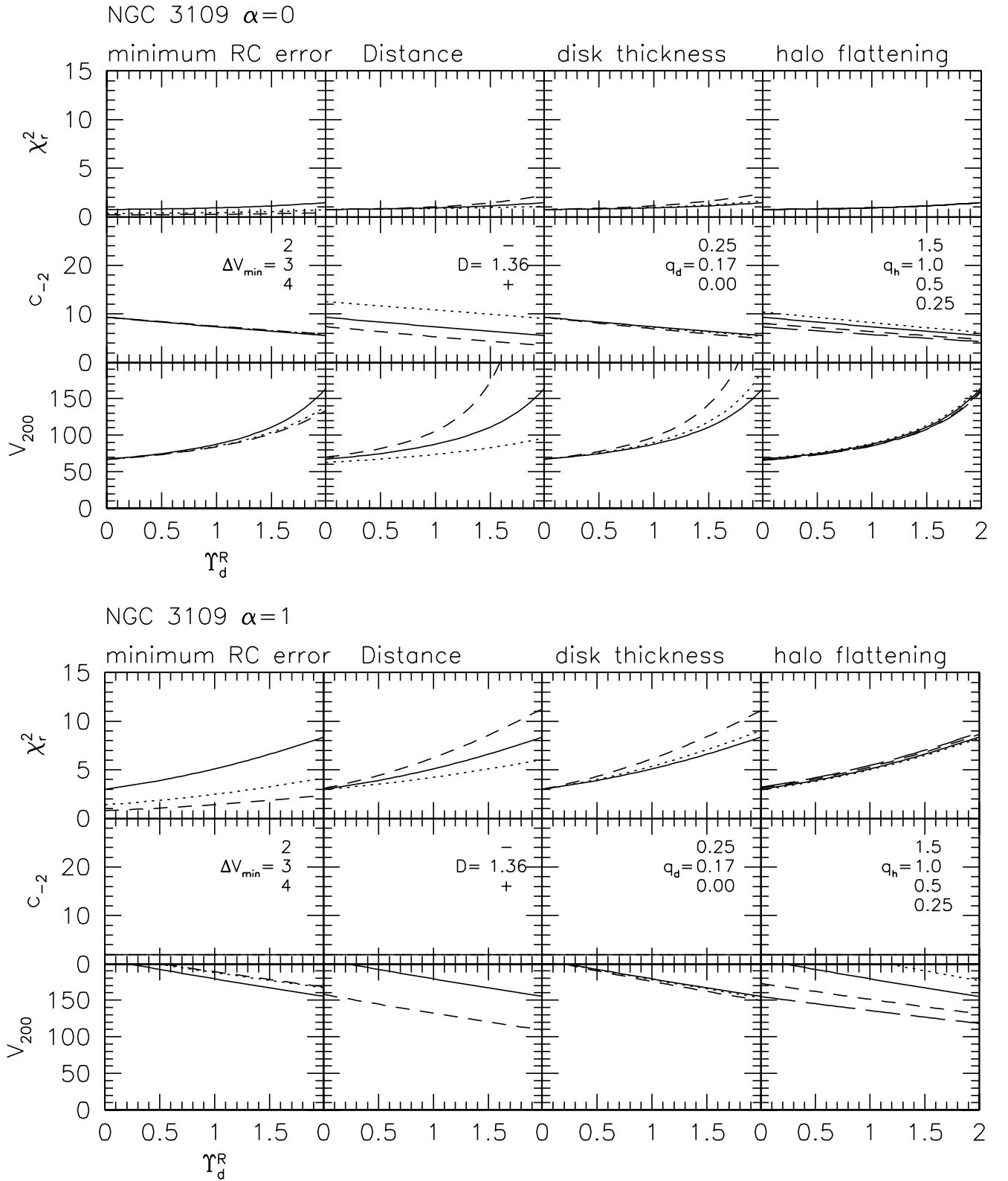


FIG. 11.— Effect of minimum rotation curve errors, distance, disk thickness, and halo flattening for  $\alpha = 0$  and 1 halos for all six galaxies. Minimum RC errors: 2 (solid line), 3 (dotted line), 4 (dashed line); Distance: adopted (solid line), -30% (dotted line), +30% (dashed line); disk thickness: 0.25 (solid line), 0.17 (dotted line), 0.00 (dashed line); halo flattening: 1.00 (solid line), 1.50 (dotted line), 0.50 (dashed line), 0.25 (long-dashed line).

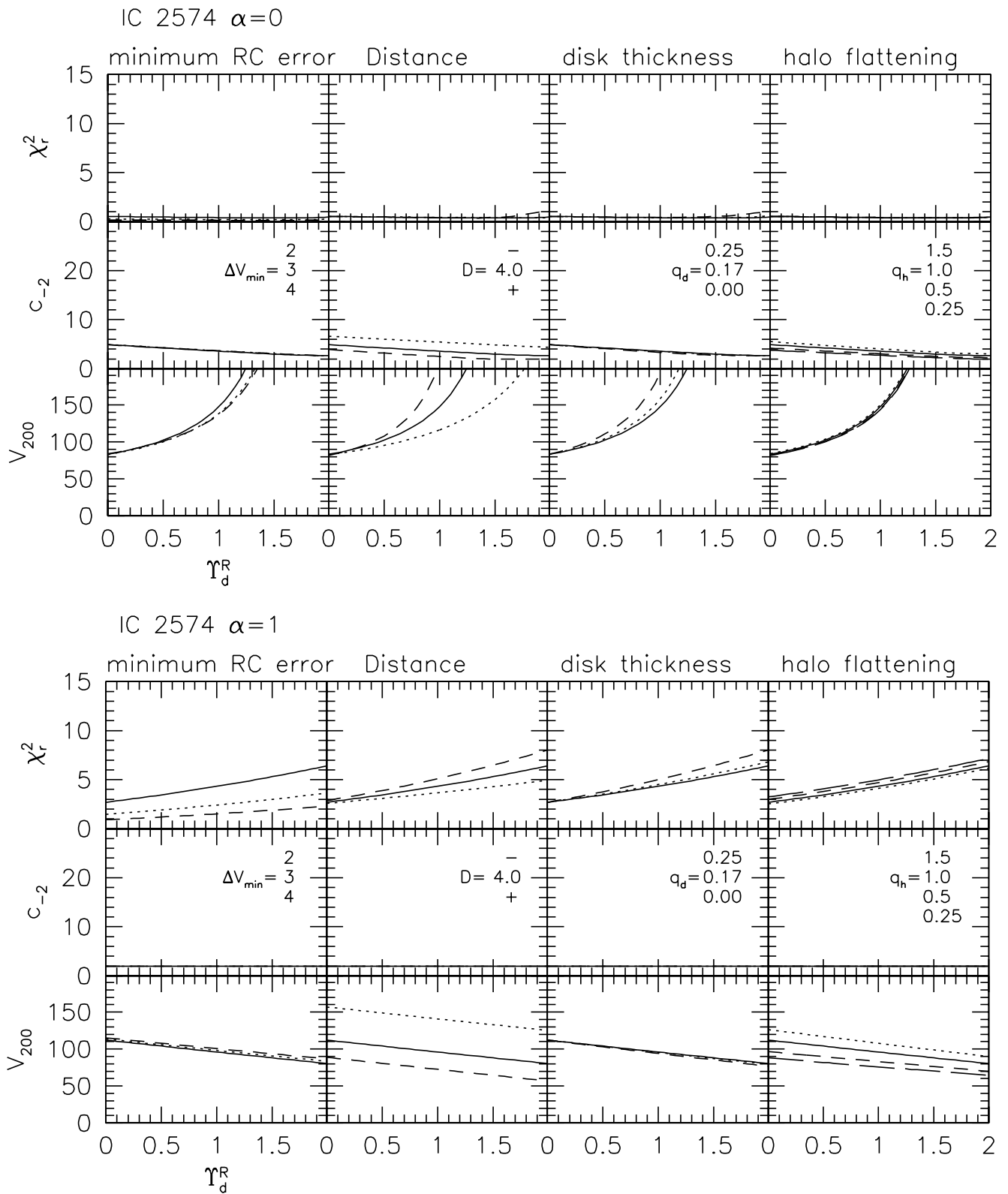


FIG. 11.— Continued.

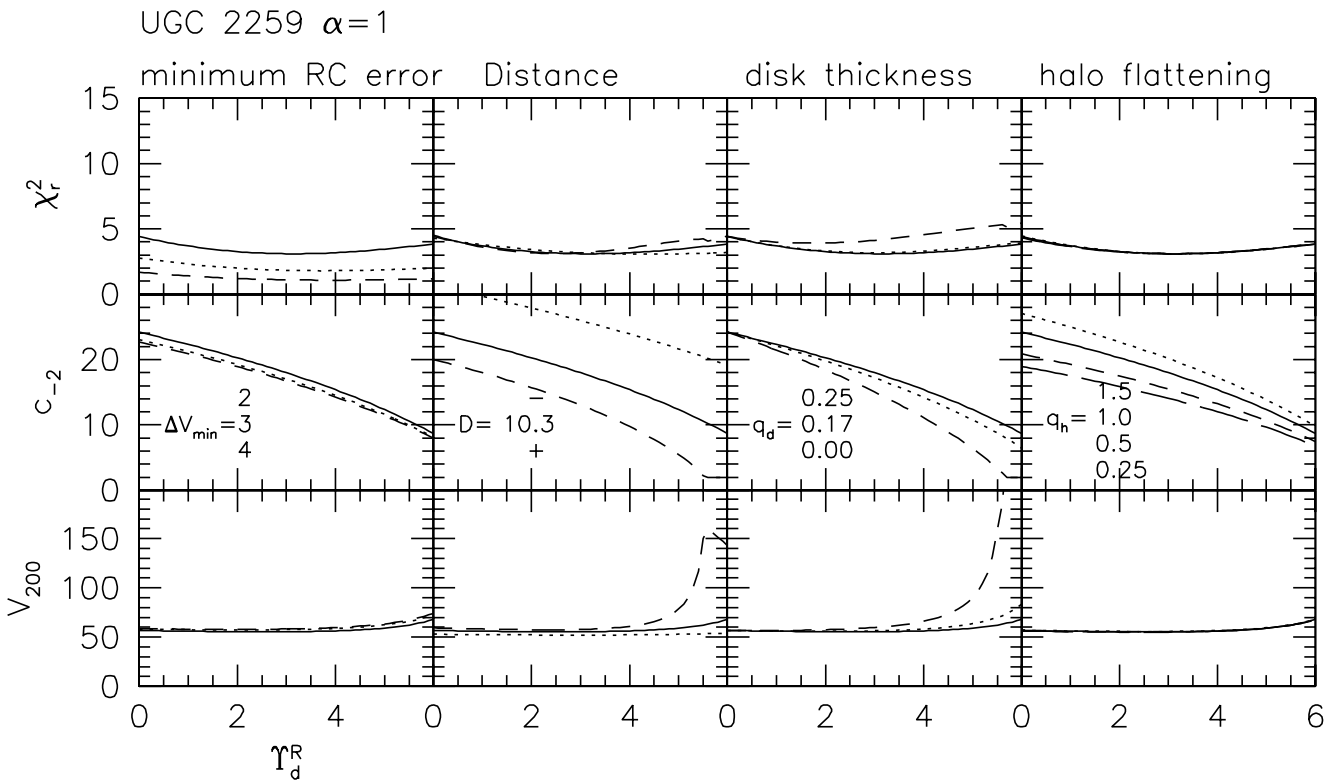
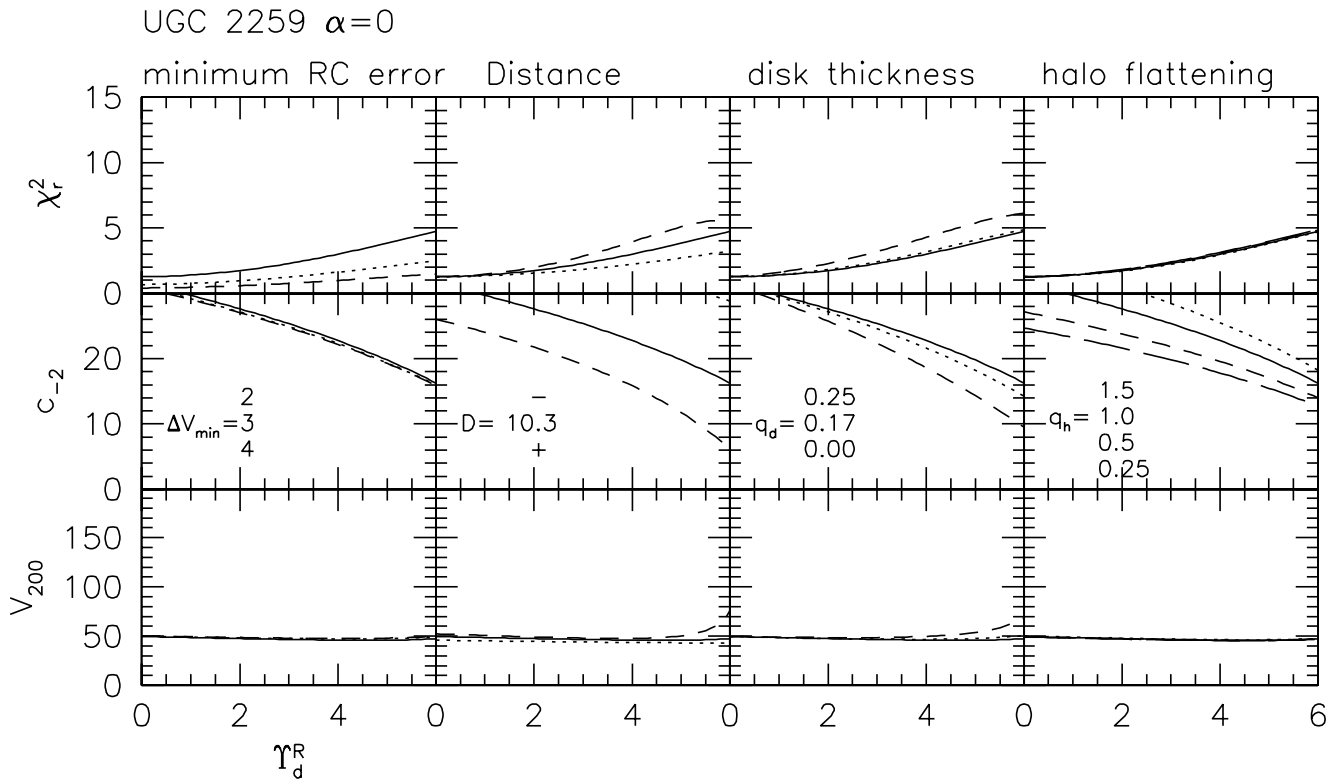


FIG. 11.— Continued.

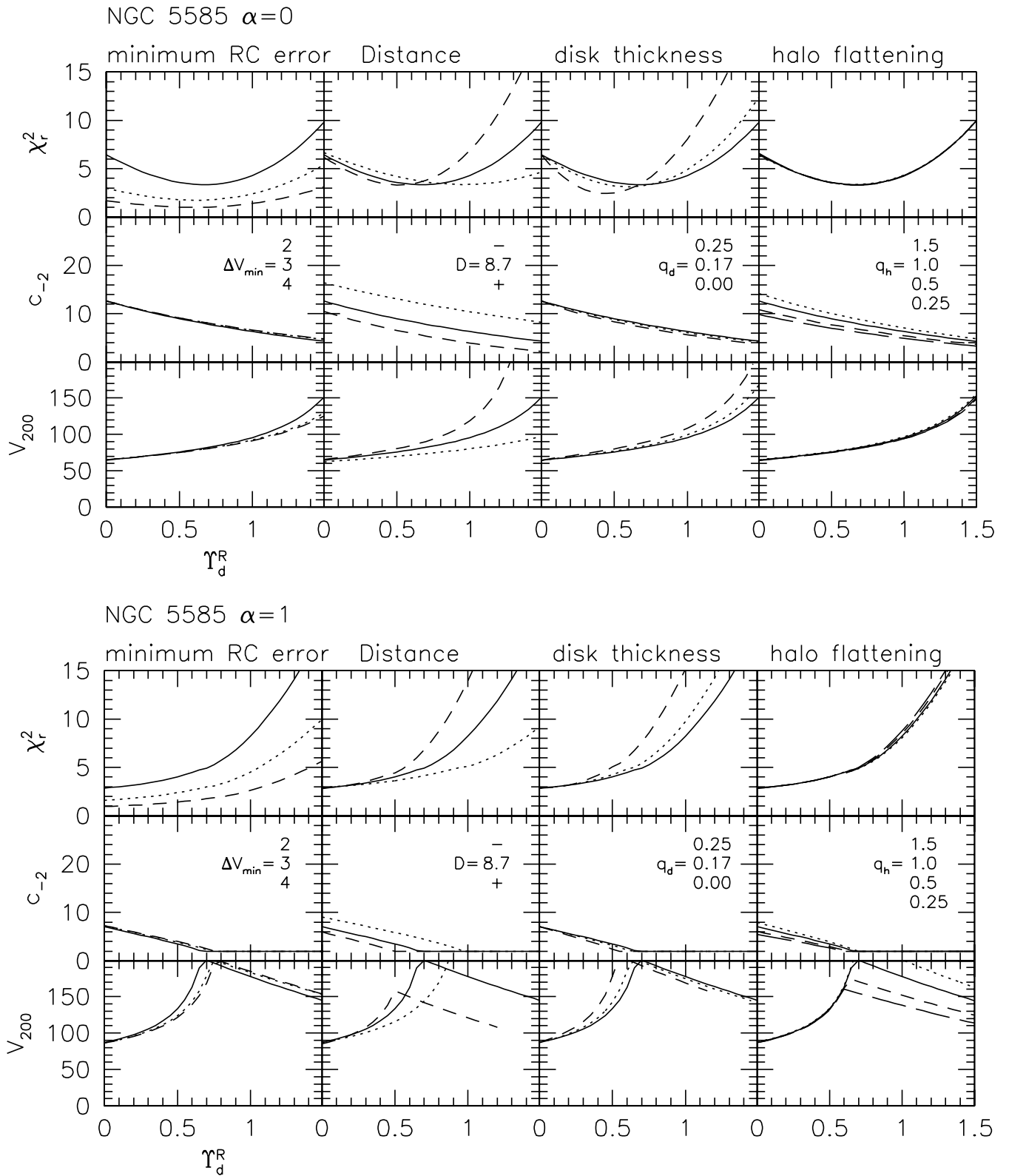


FIG. 11.— Continued.

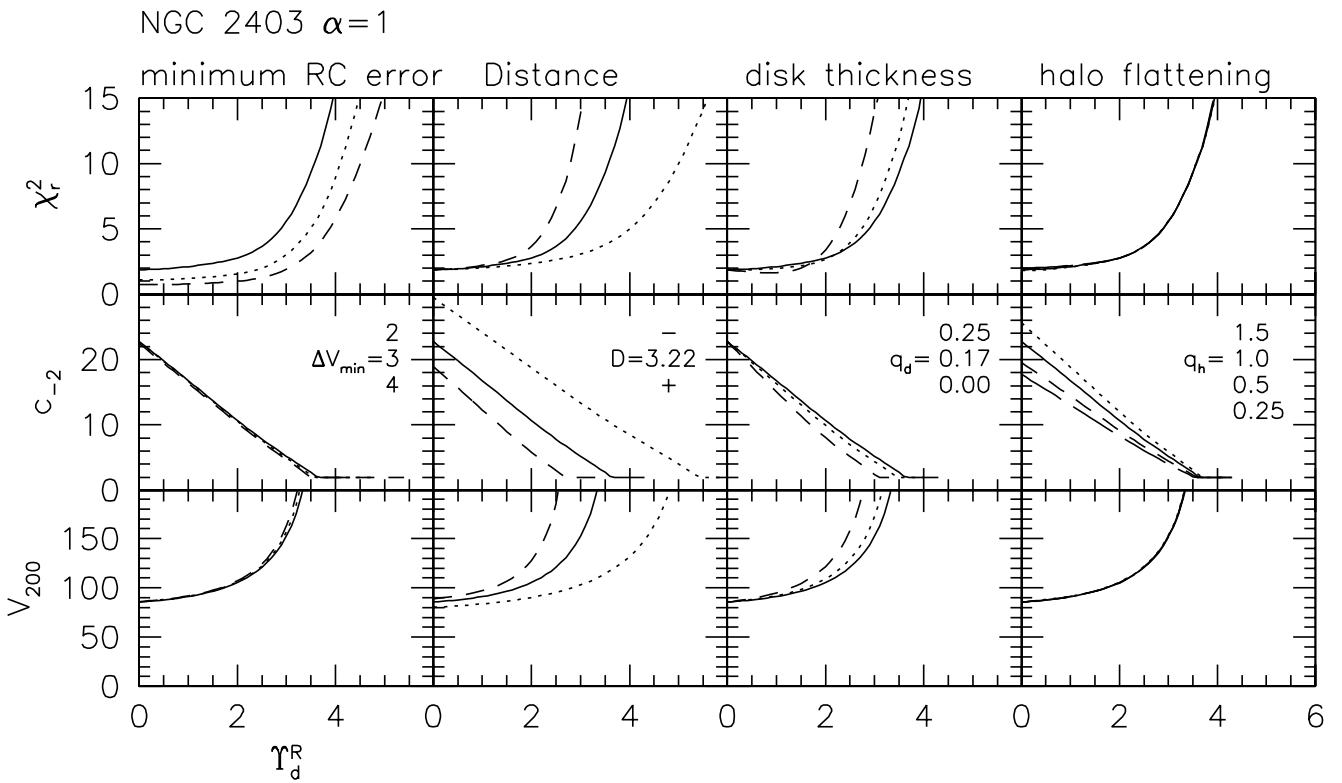
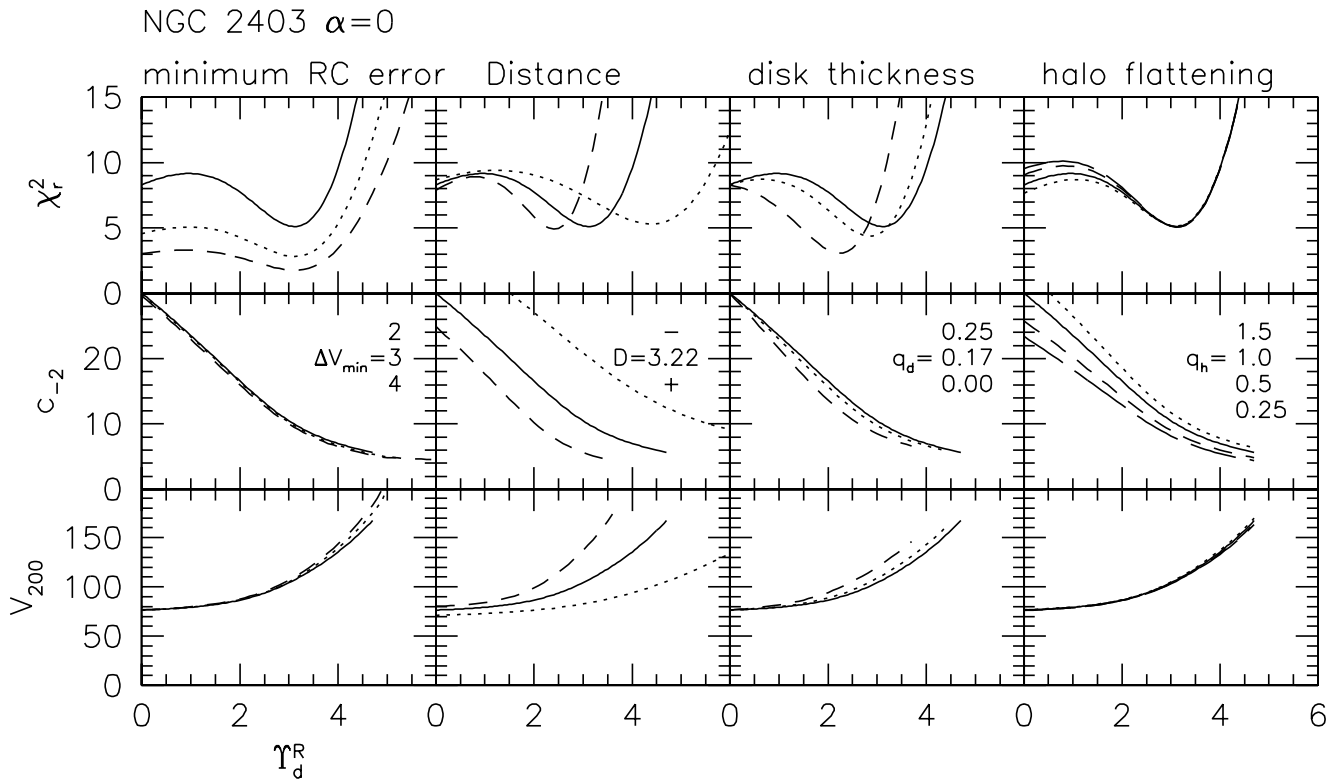


FIG. 11.— Continued.

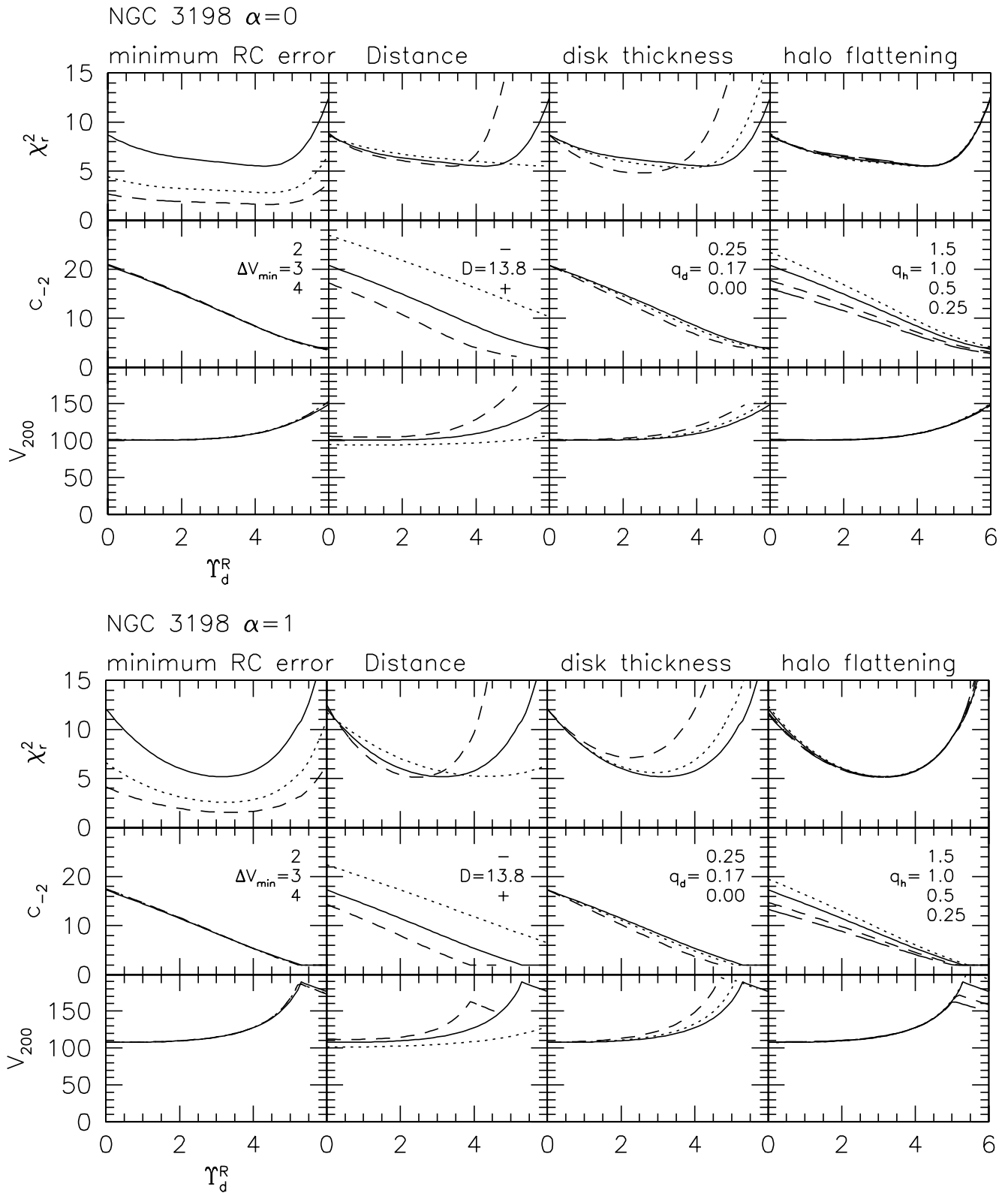


FIG. 11.— Continued.



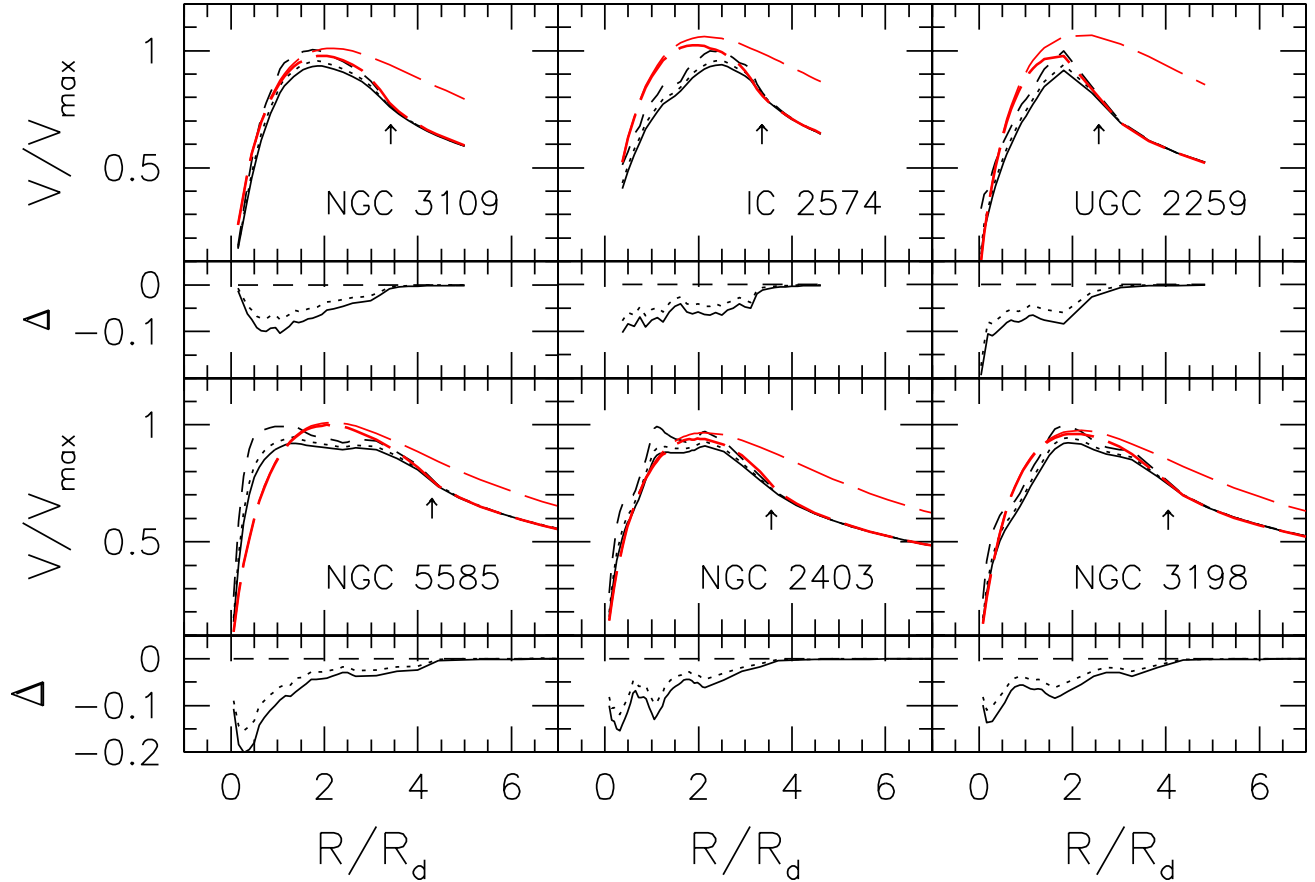


FIG. 12.— Effect of disk thickness on disk circular velocity. The rotation curves were calculated from the observed surface brightness profile, with a disk thickness  $q_d = 0$  (dashed line), 0.17 (dotted line), and 0.25 (solid line). For comparison we also show the rotation curves of exponential disks (long-dashed line) truncated at the last surface brightness data point and continued to infinity. The truncation radius is indicated by an arrow. The bottom panel shows the residuals with respect to the thin disk.

the best-fit  $\alpha = 0$ ). Our best-fit models with constraints favor sub-maximal disk models, with  $V_{\text{disk}}/V_{\text{tot}} \lesssim 0.6$  at 2.2 disk scale lengths for all six galaxies.

Accurately determining the error bars (both statistical and systematic) on the observed rotation curve(s) is crucial to breaking the degeneracies. Doubling the minimum rotation curve error values from, say, 2 to just  $4 \text{ km s}^{-1}$  reduces the differences in  $\chi_r^2$  between models with different  $\alpha$  or  $\Upsilon_d^R$  to statistically insignificant levels.

Changing the distance or disk thickness of the galaxy alters the best-fitting  $\Upsilon_d^R$ , although the relative difference in goodness of fit between  $\alpha = 0$  and  $\alpha = 1$  halos is not significant. The effect of halo flattening is to decrease its concentration, but the effect on  $\chi^2$  is practically unchanged.

Thus, given the above uncertainties, we conclude that rotation curve mass modeling of disk galaxies fails to provide tight constraints on the central density slope of dark matter halos.<sup>7</sup> Constraints on central density slopes are possibly strongest in low-mass galaxies, especially LSB galaxies, provided that there are no systematic errors in the rotation curves. Unfortunately, at present, the predictions of numerical simu-

lations for these galaxy types are the weakest.

However, the prospects for determining the relative amounts of dark and visible matter in disk galaxies (e.g., beyond  $2R_d$ , where the rotation curve becomes flatter) look more promising provided that near-IR imaging and SPS models or velocity dispersion measurements are available to constrain  $\Upsilon_d$ .

**Acknowledgements:** We would like to thank Lauren MacArthur, Joel Primack and Frank van den Bosch for helpful discussions, Matt Choptuik for use of the VN cluster at UBC, and the referee for useful comments that led to a more condensed and focused presentation. S. C. and C. C. acknowledge financial support from the National Science and Engineering Council of Canada. This research has made use of NASA's Astrophysics Data System Abstract Service, as well as the NASA/IPAC Extragalactic Database (NED), which is operated by the Jet Propulsion Laboratory, California Institute of Technology, under contract with the National Aeronautics and Space Administration.

<sup>7</sup> Similar limitations for the mass modeling of dwarf and LSB disk galaxies are addressed in Swaters et al. (2003), and for elliptical galaxies in Côté et al. (2003).

## REFERENCES

- Andersen, D. R. & Bershad, M. A. 2003, *ApJ*, 599, L79  
 Athanassoula, E. 2003, *Rev. Mex. AA Conf. Ser.*, 17, 28  
 Barnes, E. I., Sellwood, J. A., & Kosowsky, A. 2004, *AJ*, 128, 2724  
 Begeman, K. G. 1987, Ph.D. thesis, Univ. Groningen  
 Bell, E. F. & de Jong, R. S. 2001, *ApJ*, 550, 212  
 Binney, J. & Tremaine, S. 1987, *Galactic Dynamics* (Princeton, Princeton Univ. Press)  
 Bizyaev, D. & Mitronova, S. 2002, *A&A*, 389, 795  
 Blais-Ouellette, S., Carignan, C., Amram, P., & Côté, S. 1999, *AJ*, 118, 2123  
 Blais-Ouellette, S. 2000, Ph.D. thesis, Univ. Montréal and Univ. Provence  
 Blais-Ouellette, S., Amram, P., & Carignan, C. 2001, *AJ*, 121, 1952  
 Blais-Ouellette, S., Amram, P., Carignan, C., & Swaters, R. 2004, *A&A*, 420, 147  
 Blumenthal, G. R., Faber, S. M., Flores, R., & Primack, J. R. 1986, *ApJ*, 301, 27  
 Bottema, R. 1993, *A&A*, 275, 16  
 Bottema, R. 1997, *A&A*, 328, 517  
 Broeils, A. H. & Courteau, S. 1997, in *ASP Conf. Ser. 117: Dark and Visible Matter in Galaxies and Cosmological Implications*, ed. M. Persic & Salucci (San Francisco: ASP), 74  
 Bryan, G. L. & Norman, M. L. 1998, *ApJ*, 495, 80  
 Buchhorn, M. 1992, Ph.D. thesis, Australian National Univ.  
 Bullock, J. S., Kolatt, T. S., Sigad, Y., Somerville, R. S., Kravtsov, A. V., Klypin, A. A., Primack, J. R., & Dekel, A. 2001, *MNRAS*, 321, 559  
 Carignan, C. & Freeman, K. C. 1985, *ApJ*, 294, 494  
 Carignan, C., Sancisi, R., & van Albada, T. S. 1988, *AJ*, 95, 37  
 Casertano, S. 1983, *MNRAS*, 203, 735  
 Casertano, S. & van Gorkom, J. H. 1991, *AJ*, 101, 1231  
 Combes, F. 2002, *NewA Rev.*, 46, 755  
 Corradi, R. L. M., Boulesteix, J., Bosma, A., Amram, P., & Capaccioli, M. 1991, *A&A*, 244, 27  
 Côté, S., Carignan, C., & Sancisi, R. 1991, *AJ*, 102, 904  
 Côté, P., McLaughlin, D. E., Cohen, J. G., & Blakeslee, J. P. 2003, *ApJ*, 591, 850  
 Courteau, S. & Rix, H. 1999, *ApJ*, 513, 561  
 Courteau, S., Andersen, D. R., Bershad, M. A., MacArthur, L. A., & Rix, H. 2003, *ApJ*, 594, 208  
 Courteau, S., MacArthur, L. A., Dekel, A., van den Bosch, F. C., Dutton, A. A., McIntosh, D. H., Dale, D. 2005, preprint (astro-ph/0310440)  
 Debattista, V. P. & Williams, T. B. 2004, *ApJ*, 605, 714  
 Debattista, V. P. & Sellwood, J. A. 2000, *ApJ*, 543, 704  
 de Blok, W. J. G. & McGaugh, S. S. 1997, *MNRAS*, 290, 533  
 de Blok, W. J. G., McGaugh, S. S., & Rubin, V. C. 2001a, *AJ*, 122, 2396  
 de Blok, W. J. G., McGaugh, S. S., Bosma, A., & Rubin, V. C. 2001b, *ApJL*, 552, L23  
 Dekel, A., Devor, J., & Hatzroni, G. 2003, *MNRAS*, 341, 326  
 Diemand, J., Moore, B., & Stadel, J. 2004, *MNRAS*, 353, 624  
 Drozdovsky, I. O. & Karachentsev, I. D. 2000, *A&AS*, 142, 425  
 Dubinski, J. & Carlberg, R. G. 1991, *ApJ*, 378, 496  
 Dubinski, J. 1994, *ApJ*, 431, 617  
 Eke, V. R., Navarro, J. F., & Steinmetz, M. 2001, *ApJ*, 554, 114  
 Flores, R., Primack, J. R., Blumenthal, G. R., & Faber, S. M. 1993, *ApJ*, 412, 443  
 Flores, R. A. & Primack, J. R. 1994, *ApJL*, 427, L1  
 Freedman, W. L. et al. 2001, *ApJ*, 553, 47  
 Freeman, K. C. 1970, *ApJ*, 160, 811  
 Fukushige, T. & Makino, J. 2001, *ApJ*, 557, 533  
 Ghigna, S., Moore, B., Governato, F., Lake, G., Quinn, T., & Stadel, J. 2000, *ApJ*, 544, 616  
 Gnedin, O. Y., Kravtsov, A. V., Klypin, A. A., & Nagai, D. 2004, *ApJ*, 616, 16  
 Hernquist, L. & Weinberg, M. D. 1992, *ApJ*, 400, 80  
 Jesseit, R., Naab, T., & Burkert, A. 2002, *ApJL*, 571, L89  
 Jing, Y. P. & Suto, Y. 2000, *ApJ*, 529, L69  
 Jing, Y. P. & Suto, Y. 2002, *ApJ*, 574, 538  
 Jobin, M. & Carignan, C. 1990, *AJ*, 100, 648  
 Jorgensen, I. 1994, *PASP*, 106, 967  
 Karachentsev, I. D. et al. 2002, *A&A*, 383, 125  
 Katz, N. & Gunn, J. E. 1991, *ApJ*, 377, 365  
 Kent, S. M. 1987, *AJ*, 93, 816  
 Klypin, A., Kravtsov, A. V., Bullock, J. S., & Primack, J. R. 2001, *ApJ*, 554, 903  
 Kranz, T., Slyz, A., & Rix, H. 2003, *ApJ*, 586, 143  
 Kravtsov, A. V., Klypin, A. A., Bullock, J. S., & Primack, J. R. 1998, *ApJ*, 502, 48  
 Kregel, M., van der Kruit, P. C., & de Grijs, R. 2002, *MNRAS*, 334, 646  
 MacArthur, L. A., Courteau, S., & Holtzman, J. A. 2003, *ApJ*, 582, 689  
 Maller, A. H. & Dekel, A. 2002, *MNRAS*, 335, 487  
 Maller, A. H., Simard, L., Guhathakurta, P., Hjorth, J., Jaunsen, A. O., Flores, R. A., & Primack, J. R. 2000, *ApJ*, 533, 194  
 Martimbeau, N., Carignan, C., & Roy, J.-R. 1994, *AJ*, 107, 543  
 McGaugh, S. S. & de Blok, W. J. G. 1998, *ApJ*, 499, 41  
 Mo, H. J., Mao, S. 2003, astro-ph/0311459  
 Moore, B. 1994, *Nature*, 370, 629  
 Moore, B., Quinn, T., Governato, F., Stadel, J., & Lake, G. 1999, *MNRAS*, 310, 1147  
 Musella, I., Piotto, G., & Capaccioli, M. 1997, *AJ*, 114, 976  
 Navarro, J. F., Frenk, C. S., & White, S. D. M. 1996, *ApJ*, 462, 563  
 Navarro, J. F., Frenk, C. S., & White, S. D. M. 1997, *ApJ*, 490, 493  
 Navarro, J. F., Hayashi, E., Power, C., Jenkins, A. R., Frenk, C. S., White, S. D. M., Springel, V., Stadel, J., & Quinn, T. R. 2004, *MNRAS*, 349, 1039  
 Power, C., Navarro, J. F., Jenkins, A., Frenk, C. S., White, S. D. M., Springel, V., Stadel, J., & Quinn, T. 2003, *MNRAS*, 338, 14  
 Prada, F., et al. 2003, *ApJ*, 598, 260  
 Sackett, P. D. 1997, *ApJ*, 483, 103  
 Schlegel, D. J., Finkbeiner, D. P., & Davis, M. 1998, *ApJ*, 500, 525  
 Seljak, U. 2002, *MNRAS*, 334, 797  
 Swaters, R. A. 1999, Ph.D. thesis, Rijksuniversiteit Groningen  
 Swaters, R. A., Madore, B. F., & Trewella, M. 2000, *ApJL*, 531, L107  
 Swaters, R. A., Madore, B. F., van den Bosch, F. C., & Balcells, M. 2003a, *ApJ*, 583, 732  
 Swaters, R. A., Verheijen, M. A. W., Bershad, M. A., & Andersen, D. R. 2003b, *ApJ*, 587, L19  
 Tinker, J. L., Ryden, B. S. 2002, preprint (astro-ph/0209165)  
 Trott, C. M. & Webster, R. L. 2002, *MNRAS*, 334, 621  
 Valenzuela, O. & Klypin, A. 2003, *MNRAS*, 345, 406  
 van Albada, T. S., Bahcall, J. N., Begeman, K., & Sancisi, R. 1985, *ApJ*, 295, 305  
 van Albada, T. S. & Sancisi, R. 1986, *Philos. Trans. R. Soc. London*, A320, 447  
 van den Bosch, F. C., Robertson, B. E., Dalcanton, J. J., & de Blok, W. J. G. 2000, *AJ*, 119, 1579  
 van den Bosch, F. C. & Swaters, R. A. 2001, *MNRAS*, 325, 1017  
 van der Kruit, P. C. & Searle, L. 1981, *AAP*, 95, 105  
 Verheijen, M. A. W. 1997, Ph.D. thesis, Univ. Groningen  
 Verheijen, M. A. W., Bershad, M. A., Andersen, D. R., Swaters, R. A., Westfall, K., Kelz, A., & Roth, M. M. 2004, *AN* 325 151  
 Wechsler, R. H., Bullock, J. S., Primack, J. R., Kravtsov, A. V., & Dekel, A. 2002, *ApJ*, 568, 52  
 Weinberg, M. D. 1985, *MNRAS*, 213, 451  
 Weinberg, M. D., & Katz, N. 2002, *ApJ*, 580, 627  
 Weiner, B. J., Sellwood, J. A., & Williams, T. B. 2001, *ApJ*, 546, 931  
 Wilson, G., 2003, Ph.D. thesis, Australia National Univ.  
 Zhao, D. H., Jing, Y. P., Mo, H. J., & Börner, G. 2003, *ApJ*, 597L, 9